Available online at www.sciencedirect.com
ScienceDirect
Geochimica et Cosmochimica Acta 73 (2009) 3148–3170
Geochimica et Cosmochimica Acta
www.elsevier.com/locate/gca

Spatial variations in chemical weathering and CO_2 consumption in Nepalese High Himalayan catchments during the monsoon season

Domenik Wolff-Boenisch [a,*], Emmanuel J. Gabet [b], Douglas W. Burbank [c], Heiko Langner [d], Jaakko Putkonen [e]

[a] *Sierra Nevada Research Institute, University of California, Merced, CA 95344, USA*
[b] *Department of Geology, San Jose State University, San Jose, CA 95192, USA*
[c] *Department of Geological Sciences, University of California, Santa Barbara, CA 93110, USA*
[d] *Department of Geological Sciences, University of Montana, Missoula, MT 59802, USA*
[e] *Earth and Space Sciences, University of Washington, Seattle, WA 98195, USA*

Received 19 May 2008; accepted in revised form 9 March 2009; available online 20 March 2009

Abstract

The major ion chemistry of the Marsyandi basin and six of its tributaries in the Nepalese Himalaya have been investigated during the monsoon months of 2002. Weekly water samples taken at 10 river monitoring stations in the Annapurna watershed over the course of 4 months provide chemical weathering data for the region at an unprecedented temporal and spatial resolution. The river chemistry of all but one basin is heavily dominated by carbonate weathering which, compared to silicate weathering, contributes 80 to 97% of the total solute load. This prevalence is due to a combination of (a) intrinsically faster dissolution kinetics of carbonates, (b) relatively high runoff and (c) glacial meltwater and low temperatures at high altitudes resulting in enhanced carbonate solubilities. Monitoring stations with headwaters in the Tethyan Sedimentary Series (TSS) are particularly carbonate-rich and slightly supersaturated with respect to calcite through half of the monsoon season. Silicate weathering in the TSS is driven largely by sulfuric acid and therefore does not contribute significantly to the drawdown of atmospheric CO_2. With respect to the tributaries in the Greater Himalayan Sequence (GHS), carbonate weathering is practically as predominant as for the TSS, in spite of the largely felsic lithology of the GHS. Relative to the TSS, the primary proton source in the GHS has shifted, with at least 80% of the protons derived from carbonic acid. Averaged over the whole field area, the CO_2 fluxes, based on silicate-derived Ca and Mg, are considerably lower than the global average. Assuming that this study area is representative of the entire range, we conclude that *in situ* weathering of the High Himalayas does not represent a significant sink of atmospheric carbon dioxide, despite the presence of a watershed south of the GHS that is characterized by a four times higher CO_2 consumption rate than the global average. Silicate weathering rates of all basins appear to be climate controlled, displaying a tight correlation with runoff and temperature. Given the extremely low chemical weathering under transport-limited conditions in high-altitude crystalline terrains outside of the monsoon season, this would result in virtually no chemical exhumation for 2/3 of the year in such a cold and arid climate, north of the rain shadow cast by the High Himalayas.
© 2009 Elsevier Ltd. All rights reserved.

1. INTRODUCTION

The weathering of silicate minerals coupled with subsequent carbonate precipitation leads to the drawdown of atmospheric CO_2 and provides a natural counterbalance to volcanic activity that releases huge quantities of this

* Corresponding author. Address: Domenik Wolff-Boenisch, University of Iceland, Sturlugata 7, 101 Reykjavik, Iceland.
E-mail address: boenisch@raunvis.hi.is (D. Wolff-Boenisch).

0016-7037/$ - see front matter © 2009 Elsevier Ltd. All rights reserved.
doi:10.1016/j.gca.2009.03.012

greenhouse gas into the atmosphere. The quantitative relationship between weathering and CO_2 consumption and the implications for the global climate have attracted much scientific attention, especially as it became evident that anthropogenic activity surpassed volcanic activity in the emission of CO_2 (e.g., Gerlach, 1991), thus imposing an imbalance on this climatic coupling. Of interest are the principal factors that govern the magnitude of silicate weathering. Past studies reveal that climatic parameters such as precipitation/runoff, temperature, and vegetation exert important controls on the chemical weathering of silicates (Velbel, 1993; Bluth and Kump, 1994; White and Blum, 1995; Anderson et al., 1997; White et al., 1999a; Moulton et al., 2000; Dessert et al., 2001; Berner et al., 2003; Dupré et al., 2003; France-Lanord et al., 2003; Das et al., 2005; West et al., 2005). However, physical erosion has also been found to be closely linked to chemical weathering (Bluth and Kump, 1994; Stallard, 1995; Gaillardet et al., 1997, 1999; Krishnaswami et al., 1999; Riebe et al., 2001a,b, 2003, 2004a,b; Dalai et al., 2002a; Millot et al., 2002; West et al., 2002, 2005; France-Lanord et al., 2003; Jacobson et al., 2003; Singh et al., 2005; Lyons et al., 2005; Gabet, 2007). Finally, the role of lithology in climate forcing may be important as well (Stallard and Edmond, 1983; Jha et al., 1988; Bluth and Kump, 1994; Jenkins et al., 1995; Edmond et al., 1996; Louvat and Allegre, 1997; Huh et al., 1998; Gaillardet et al., 1999; English et al., 2000; Amiotte-Suchet et al., 2003; Dessert et al., 2003; Dupré et al., 2003).

Consequently, more recent studies propose a combined approach whereby silicate weathering is governed by climatically controlled chemical denudation under circumstances of high material supply and fast removal processes (kinetically limited) and by erosionally controlled chemical weathering in times of low material supply and slow removal processes (transport limited) (e.g., Riebe et al., 2004a; West et al., 2005; Gabet and Mudd, 2009). Riebe et al. (2004b) found that chemical weathering rates are particularly sensitive to differences in climate at higher-altitude sites and fall virtually to zero at the highest altitudes in their study. To the extent that chemical weathering rates are supply limited in mountainous landscapes, factors that regulate rates of mineral supply from erosion, such as tectonic uplift, may lead to significant fluctuations in global climate over the long term. This link between tectonics and climate has led to many studies in the Himalayan Orogen to examine whether tectonic uplift on a regional scale and subsequent erosion can cause enhanced CO_2 consumption and cooling on a global scale (e.g., Raymo and Ruddiman, 1992; France-Lanord and Derry, 1997).

The Himalayas provide an ideal backdrop for weathering-related studies because they combine steep temperature and precipitation gradients with marked morphological relief and the juxtaposition of varying lithological terrains. They also pose the formidable task of interpreting trunk stream chemistry data as a function of these varying parameters, especially when considering the temporal variations in major element (and isotope) chemistry due to seasonal precipitation and the spatial variations in lithology. Before a full accounting of the controls on chemical weathering can be made, however, it is critical to look closely at the geochemical processes at work. Only after an in-depth analysis of the river chemistry in the light of contributions from rain, hydrothermal and/or human activity, disseminated calcite or the principal proton source, can the underlying interplay of climate and erosion on weathering rates be revealed. In this contribution, we describe our results and interpretations from monitored watersheds in the High Himalayas of Nepal. Whereas others have previously examined similar issues in the Himalayas (e.g., Krishnaswami and Singh, 1998; Galy and France-Lanord, 2001), the work presented in this contribution represents a step forward for several reasons. First, water samples were collected at a higher spatial and temporal density than in previous studies, thus allowing for a detailed analysis of the geochemical processes and the calculation of weathering rates with a greater level of accuracy. Second, we pair solute concentrations with discharge measurements to calculate solute fluxes; a recent study from the same watershed (Tipper et al., 2006) did not have the benefit of river flow measurements. Third, silicate and carbonate weathering rates are adjusted according to the spatial extent of the source rocks. This approach provides a more accurate estimate of weathering rates than simply dividing the solute discharge by the total area, which can only provide minimum weathering rates. Finally, the watersheds studied here are generally at higher altitudes than in previous studies (e.g., Dalai et al., 2002a), thus extending the solute data set from the Himalayas into the colder regions.

In the present study, emphasis has been placed on studying a relatively constrained catchment area in central Nepal during the monsoon season. It is one of the wettest and fastest eroding regions in the High Himalayas (Lavé and Avouac, 2001; Burbank et al., 2003) and thus provides insight into chemical weathering processes under entirely kinetically limited conditions during the monsoon season. Since seasonal variations have been precluded (by looking strictly only at data from the rainy season) but runoff/discharge is high, an interpretation of the river chemistry based on lithology is presented. Following a quantification and assessment of chemical weathering rates in the central Himalaya, we examine weathering controlled CO_2 consumption rates in the light of climate forcing.

2. STUDY AREA

The watersheds in this study lie within the Himalayan Annapurna–Manaslu massifs, Nepal (Fig. 1). This area is drained by the Marsyandi River, whose headwaters originate in the Tethyan Sedimentary Series (TSS). On its way southeast, the Marsyandi traverses the Greater Himalayan Sequence (GHS; also referred to as High Himalaya Crystalline Series, HHCS), before bending south and incising through the Lesser Himalayan Sequence (LHS). Because the Marsyandi and its tributaries drain different regions within this part of the Himalaya, a closer look at the underlying lithology is required. The following geologic description is based on Gleeson and Godin (2006) and Upreti (1999) and references cited therein. Note that the transition zone between TSS and GHS (viz. the South Tibetan

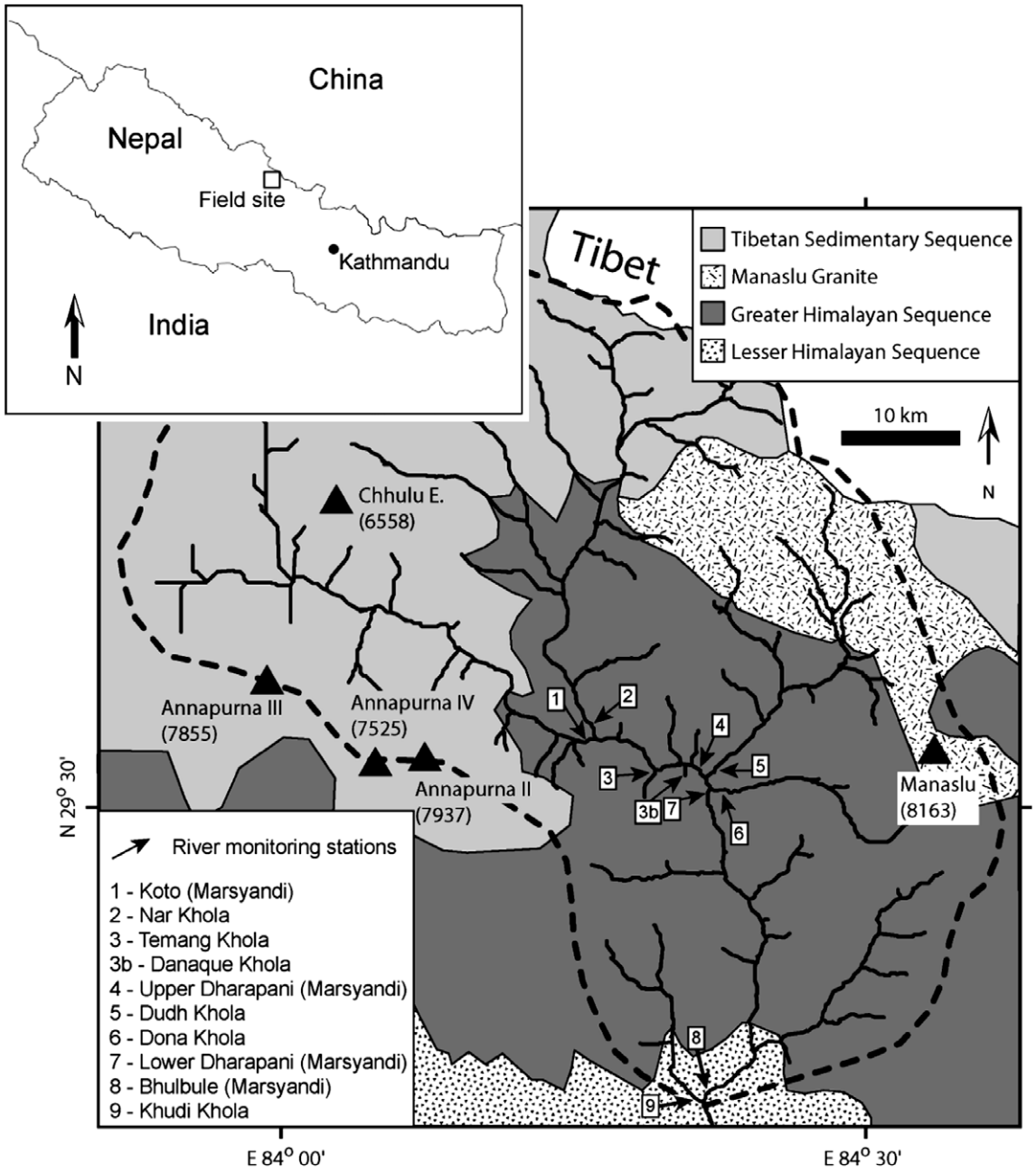

Fig. 1. Lithological map (modified from Searle and Godin, 2003) of the study area depicting the locations of river monitoring stations. Site names are shown in the legend. Dashed line = watershed boundary.

Detachment System) as well as the contact between GHS and LHS (viz. the Main Central Thrust, MCT) have been omitted in this description. These are geologic features of tectonic relevance but with similar lithology as the main sequences and thus of minor importance in this study.

The Tethyan Sedimentary Series is characterized by Cambro-Ordovician to Tertiary sediments. These sediments are subdivided into different formations according to their age consisting of (from old to new) mica-schist, metamorphosed and unmetamorphosed sandstone, fossil-rich limestone, quartzite including calcareous arkose and siltstone, black shale, limestone and a massive carbonate sequence. Part of the TSS is covered by glaciers and hence glacial meltwater contributes to the water volume of streams in this catchment area.

The Greater Himalayan Sequence is distinguished from the TSS by the higher grade of metamorphism and deformation. The GHS consists of Proterozoic to Palaeozoic sedimentary and granitic rocks, metamorphosed at amphibolite to granulite facies. Three major units have been distinguished. Unit I consists of interlayered kyanite–sillimanite grade pelitic schist, gneiss and migmatite.

The dominant lithology of Unit II is a calc-silicate gneiss with dark diopside-hornblende-biotite rich layers and light quartz–feldspar–calcite rich layers. It also includes marble. Unit III is an interlayered biotite schist and orthogneiss. Adding to this complex and varied lithology, synmetamorphic leucogranites, including the Manaslu leucogranite and various smaller bodies and dykes, intrude the GHS and TSS.

The Lesser Himalayan Sequence, in which mainly Precambrian rocks are involved, is made up of low-grade metasedimentary rock units, with overriding crystalline nappes. The units consist of schist, phyllite, gneiss, quartzite, granite and limestone. Marbles occur at the northern edge of the LHS.

3. DATA ACQUISITION AND PROCESSING

3.1. Sampling and analysis

Between 2000 and 2001, 10 river monitoring stations were established along the Marsyandi River and selected tributaries (Fig. 1), covering an overall catchment area of $\sim$3400 km^2. These sites overlapped with a network of meteorological stations that had been previously installed by our research group (Putkonen, 2004). The river monitoring stations were used from 2000 to 2002 to measure discharge and collect suspended sediment samples twice daily during the monsoon season (Gabet et al., 2004). In 2002, weekly water samples were also collected for chemical analyses. The Marsyandi was sampled at stations #1, 4, 7, and 8 (denoted by the suffix '-M' and being grouped together throughout this paper). Station #1 drains the TSS (TSS-M) while #4 and 7 flow over GHS lithology (summarized as GHS-M). Monitoring station #8 lies south of the MCT on LHS terrain (LHS-M). All other numbers represent sampled tributaries (suffix '-TR') of the Marsyandi where, analogously, #2 drains the TSS (TSS-TR), #3, 3b and 6 reflect GHS lithology (summarized as GHS-TR), and #9 lies in the LHS (LHS-TR). Station #5 drains not only the GHS but also the Manaslu Granite (GHS*-TR). Based on the bedrock, there are three distinct groups: #1 and 2 with headwaters in the TSS, # 8 and 9 sampled south of the MCT in the LHS, and the bulk #3–7 mirroring GHS geology. Despite being sampled within the LHS, it is noteworthy that <10% of the catchments of sites 8 and 9 encompass Lesser Himalayan rocks. This influence from GHS lithology notwithstanding, their affiliation to the LHS was chosen to highlight the change in the major lithological unit that takes place down the length of the Marsyandi.[1]

[1] The numbering scheme in this study differs systematically from the one utilized in a closely related paper (Gabet et al., 2008). The difference follows from the fact that watershed #3b in this study corresponds to #4 in Gabet et al. (2008) with the implications for all following watersheds. While we treat the very same basins as the cited study, our numbering ends at 9 while theirs end at 10. This distinction in the numbering was introduced to emphasize the similarities in lithology and watershed size and the geographic proximity of #3 (Temang) and #3b (Danaque).

The predominant geological formation of the GHS group is Unit II based on the map of Colchen et al. (1986). The main tributary #2 displays features far more comparable in size and trend to the trunk stream, and hence it will always be excluded when generalized statements about tributary chemistry are made. Table 1 presents the most important aspects of each monitoring station, such as elevation, surface area of the associated catchment, and percentage area glacierized (i.e., presently occupied by glaciers).

The weekly water samples were collected from the river in 500 ml acid-washed polyethylene (PE) bottles that had been pre-rinsed with river water. The suspended sediment was allowed to settle for $\sim$15 min. From the top of this volume, two aliquots of 50 ml were extracted using a polypropylene 0.45-μm filter attached to a syringe that had been pre-rinsed. The aliquots were stored in 50-ml acid-washed PE bottles, and subsequently one bottle was acidified with nitric acid to pH $\sim$ 1 for cation analysis.

All chemical analyses were conducted in the Environmental Science Department at the University of California, Riverside. Cations were determined through inductively-coupled plasma optical emission spectrometry (ICP-OES; Perkin-Elmer Optima 3000DV) against external standards. Relative standard deviations of replicate measurements of spiked lab blanks ($n = 23$), CCV (continuing calibration verifications, $n = 25$), and two different IPC (internal performance check solutions, $n = 11$ and 34) were less than 7%. Anions were measured on a Dionex 500 ion chromatograph (IC), using an IonPac AS11-HC (4 × 250 mm) analytical column. On the IC, the recovery of an external standard was between 94 and 106% ($n = 21$) for chloride, fluoride, and sulfate and the relative standard deviation of the difference between duplicates was 4% ($n = 18$). Given the range of uncertainties for the ICP-OES and IC measurements, we assume an overall analytical error of 10% for the concentration values. Laboratory titration to pH 4.5 with 0.16 M sulfuric acid using a Hach Kit (Model AL-DT) yielded alkalinity values as $CaCO_3$. Table 2 summarizes for each stream the major ion chemistry and discharge over the monsoon period. Given that Tipper et al. (2006) sampled the monitoring stations #1 and 2 on the same days during the same monsoon season as this study, it is possible to compare values in Table 2 with the ones given in their paper. Agreement for the key parameters Ca, Mg, and SO_4 is usually within 10%. HCO_3 values could not be compared because Tipper et al. (2006) determined them by charge balance.

3.2. Corrections and errors

Two external sources can significantly influence the river's elemental composition. First, the contribution from meteoric salts must be compensated. This is done by subtracting the composition of rain water from the river chemistry. Rain water was sampled on a biweekly basis during the 2002 monsoon season but, unfortunately, many of the samples appeared to have been mislabeled and, thus, could not be trusted. Consequently, meteoric contributions are based on only two samples that were subsequently

Table 1
Characterization of the drainage basins.

Station[a]	Basin #	Lithology[b]	A_{tot}[c] (km^2)	A_{sil}[c] (km^2)	A_{sil}/A_{tot} (%)	Elevation (m)	Relief[d] (m)	Runoff (m/y)	A_{gl}[c] (%)	T_{air}[e] (°C)
Temang	3	GHS	21	15	71	4087	1070	1.62	0	7
Nar	2	TSS	1052	889	84	5174	909	0.15	10	1
Koto M	1	TSS	812	705	87	4794	1076	0.76	12	3
Danaque	3b	GHS	7	5	71	3349	442	1.17	0	11
Upper M	4	GHS	1946	1461	75	4918	886	0.56	11	3
Lower M	7	GHS	2605	2241	86	4870	947	0.44	12	3
Dudh	5	GHS*	491	423	86	4694	1147	0.72	15	4
Dona	6	GHS	156	129	83	4851	1117	1.09	21	3
Khudi	9	LHS	152	142	93	2566	862	3.54	0	15
Bhulbule M	8	LHS	3217	2804	87	4522	958	0.76	10	5

[a] The letter 'M' indicates monitoring stations on the Marsyandi River.
[b] TSS = Tethyan Sedimentary Sequence; GHS(*) = Greater Himalayan Sequence (*including the Manaslu Granite); LHS = Lesser Himalayan Sequence.
[c] A_{tot}, A_{sil}, and A_{gl} represent the total surface area, the surface area occupied by silicates and the glacierized area, respectively.
[d] Relief calculated over a 1-km window.
[e] Mean air temperature.

combined (Table 2, last row). Nevertheless, our values are very similar to the rainwater data by Galy and France-Lanord (1999) for the Nepalese Himalaya, suggesting that our rainwater corrections are legitimate. Second, hydrothermal activity has been observed in the Marsyandi watershed with numerous hot springs located in the vicinity of the GHS/LHS divide (Evans et al., 2001, 2004). Table 2 shows that all but one catchment display low Cl concentrations in the range of tens of μM indicating that hot spring inputs to these watersheds are insignificant. Considering that Evans et al. (2001) reported a Cl concentration of ~30 mM in hot springs in the Marsyandi region, only ⩽4‰ of this hydrothermal flux may have contributed Cl to the total Cl found in all but one stream in this study. This low contribution is due to the considerable dilution of the increased spring flux by the larger increase in overall discharge during the monsoon (Evans et al., 2004). This is apparent in Table 2 where Cl concentrations of every catchment consistently increase towards the end of the monsoon when discharge and hence dilution of spring water decreases. The only monitoring station which bears signs of influx from a hot spring throughout the rainy season is #8; together with #9 it is located closest to the MCT which explains the hydrothermal contamination (Hodges et al., 2004). To be consistent and to account for the increasing Cl concentration towards the end of the monsoon season, the data from all the stations, including those with apparently low Cl concentrations, were corrected for potential hydrothermal influx. Tipper et al. (2006) provide cation/Cl ratios to subtract from measured (and rainwater-corrected) cation/Cl ratios in order to account for hydrothermal input. These molar ratios are 0.16, 0.03, 0.10, 0.41, and 0.01 for the elements Ca, Mg, K, Na, and Si, respectively.

Further simplifications were introduced to calculate silicate weathering rates and the contribution of silicates to the overall chemical weathering. These assumptions follow the ones suggested by Galy and France-Lanord (1999). After atmospheric and hot spring corrections (elements marked with a star), all of the remaining Cl is assumed to come from the dissolution of halite.[2] Subtracting this Cl* concentration from Na* yields Na_s, the silicate component of Na*. K* is assumed to be produced exclusively from silicate dissolution, therefore K* is equivalent to K_s. No contribution from the dissolution of carbonates to these alkali metals is assumed. With respect to Ca and Mg, both alkaline earths consist of a carbonate (Ca_c, Mg_c) and silicate moiety (Ca_s, Mg_s). The determination of Ca_s and Mg_s, respectively, is commonly based on the (Ca/Na) and (Mg/X) ratio (X = Na or K) of the prevailing silicate minerals and rocks encountered in the watershed, where $Ca_s = Na_s \cdot (Ca/Na)$ and $Mg_s = X_s \cdot (Mg/X)$. The problem arises in assessing a representative estimate of this elemental silicate ratio in catchments of varying lithology. Krishnaswami and Singh (1998) employed a ratio of 0.7 for Ca/Na while Jacobson et al. (2002) calculated an average Ca/Na ratio of only 0.18. These values illustrate the range of Ca/Na ratios discussed in the literature for Himalayan watersheds (cf. Hodson et al., 2002). In this study, we use Ca/Na and Mg/K ratios derived from X-ray fluorescence analysis (XRF) of suspended sediments from the respective monitoring stations (Table 3). The suspended sediments were collected as part of a parallel study on physical erosion rates; the samples were collected twice daily from the rivers by dipping weighted sample bottles into the middle of the flow (Gabet et al., 2008). Although this approach yields elemental ratios not necessarily representative of the bedrock (e.g., because the suspended material might be weathered), the Ca/Na values thus determined correspond well to the aforementioned variation found in

[2] This assumption is corroborated by a plot of the rainwater corrected elements Na vs. Cl from catchment #8, which yields a correlation coefficient r^2 of 0.97 and a slope of 1.13 ($n = 19$).

Table 2
Sampling details and chemical composition of the streams at the monitoring stations.

Sample	Date	Discharge (m^3/sec)	F (M)	Cl (M)	SO_4 (M)	NO_3 (M)	HCO_3 (M)	Ca (M)	K (M)	Mg (M)	Na (M)	Si (M)	TDS[a] (mg/L)	X_{sil}[b] (eq%)
Temang (#3)														
T-1	7/4	6.1	4	11	46	20	558	289	20	13	25	43	38	0.10
T-2	7/11	3.9	7	11	67	1	638	387	20	17	56	59	48	0.17
T-3	7/18	3.3	6	23	79	1	697	462	24	19	47	65	55	0.10
T-4	7/25	5.6	7	9	71	1	638	378	20	16	30	62	47	0.10
T-5	8/1	5.0	6	28	62	2	518	440	21	17	66	66	47	0.13
T-6	8/8	3.7	5	24	63	4	598	421	22	15	59	57	48	0.13
T-7	8/15	5.3	5	12	62	6	618	361	20	15	33	60	45	0.11
T-8	8/22	7.3	4	8	40	1	558	312	17	13	27	55	39	0.11
T-9	8/29	3.6	5	12	64	6	558	369	20	16	32	60	44	0.10
T-10	9/5	3.9	5	10	59	34	618	355	20	15	32	61	45	0.11
T-11	9/12	3.0	7	11	84	3	678	408	23	18	40	67	52	0.12
T-12	9/19	3.1	7	12	77	23	658	379	21	16	40	65	50	0.12
T-13	9/26	3.3	7	12	81	23	638	388	23	17	38	64	50	0.12
T-14	10/3	2.3	8	NA	107	30	697	443	24	20	77	72	57	0.20
T-15	10/10	2.3	10	39	122	18	877	508	27	22	88	74	69	0.15
Nar (#2)														
N-1	7/15	13.5	10	10	636	ND	1217	993	32	404	95	31	154	0.06
N-2	8/1	17.2	6	10	469	1	1257	988	27	368	96	29	138	0.06
N-3	8/7	13.5	9	9	771	ND	1257	1150	27	517	116	34	178	0.06
N-4	8/14	16.6	8	11	873	1	1377	1197	29	539	116	35	194	0.06
N-5	8/21	15.3	7	22	929	ND	1397	1249	30	579	147	35	204	0.06
N-6	8/28	15.3	9	12	1294	ND	1537	1462	30	775	153	43	257	0.06
N-7	9/3	14.8	9	14	1335	ND	1557	1469	31	819	168	45	263	0.06
N-8	9/9	10.7	9	26	1324	ND	1716	1551	31	896	198	53	274	0.06
N-9	9/16	9.1	10	27	1216	ND	1716	1469	31	836	183	53	258	0.06
N-10	9/23	6.8	11	16	1299	1	1916	1602	34	960	172	67	281	0.06
N-11	9/29	6.0	11	17	1299	32	1896	1569	33	940	170	66	279	0.06
N-12	10/5	5.7	10	19	1245	1	1816	1483	31	871	162	65	266	0.06
N-13	10/12	4.2	11	18	1410	24	1836	1495	34	1019	183	74	288	0.06
N-14	10/19	4.2	12	21	1410	31	1776	1454	35	1044	192	76	286	0.06
N-15	10/26	3.4	12	38	1390	41	1896	1480	36	1021	225	76	289	0.07
N-16	10/31	2.9	13	38	1433	27	1756	1425	35	1046	223	78	287	0.07
Koto (#1)														
KO-1	7/5	93.0	2	22	381	25	1257	841	38	300	69	29	122	0.07
KO-2	7/12	102.8	2	31	297	11	1237	767	32	225	87	25	109	0.09
KO-3	7/19	82.5	3	28	402	ND	1357	852	32	301	79	30	128	0.07
KO-4	7/26	96.8	10	23	796	ND	1257	1084	33	473	136	35	178	0.10
KO-5	8/1	75.0	4	44	499	38	1237	889	33	316	87	34	137	0.06
KO-6	8/14	90.0	3	35	510	44	1377	913	39	355	116	37	145	0.10
KO-7	8/21	120.0	3	31	603	ND	1437	936	31	350	116	36	155	0.09

(*continued on next page*)

Table 2 (*continued*)

Sample	Date	Discharge (m^3/sec)	F (M)	Cl (M)	SO_4 (M)	NO_3 (M)	HCO_3 (M)	Ca (M)	K (M)	Mg (M)	Na (M)	Si (M)	TDS[a] (mg/L)	X_{sil}[b] (eq%)
KO-8	8/28	69.8	3	33	632	7	1477	1004	31	453	101	44	165	0.07
KO-9	9/3	59.3	26	40	795	14	1577	1024	31	457	112	45	185	0.07
KO-10	9/9	36.0	3	49	654	16	1637	1029	31	510	143	52	176	0.08
KO-11	9/16	32.3	4	53	647	1	1696	1058	33	524	146	54	179	0.08
KO-12	9/23	24.8	4	43	663	4	1657	1094	33	572	122	62	182	0.07
KO-13	9/29	27.8	4	45	627	1	1756	1101	35	546	123	62	181	0.07
KO-14	10/5	24.0	4	50	697	27	1836	1047	35	592	139	65	190	0.08
KO-15	10/12	17.3	4	59	714	1	1836	1114	37	626	151	67	196	0.08
KO-16	10/19	15.0	4	62	726	37	1876	1116	37	655	157	69	200	0.08
KO-17	10/26	12.0	5	80	737	21	1916	1141	37	673	194	71	205	0.09
KO-18	10/31	10.5	5	83	742	56	1876	1113	39	670	202	74	204	0.09
Danaque (#3b)														
DQ-1	7/4	1.1	4	11	40	2	678	365	20	15	21	61	45	0.07
DQ-2	7/11	0.6	3	7	37	4	558	425	22	17	25	69	44	0.09
DQ-3	7/18	0.6	7	16	59	9	678	446	25	17	34	72	51	0.09
DQ-4	7/25	0.9	4	5	34	6	717	397	20	16	22	69	47	0.09
DQ-5	8/1	0.9	4	28	40	10	817	476	24	16	69	70	56	0.14
DQ-6	8/8	0.9	3	17	46	1	737	440	25	16	56	73	52	0.14
DQ-7	8/15	1.0	3	13	42	1	717	460	28	18	35	69	51	0.11
DQ-8	8/22	2.3	4	13	32	1	737	454	34	19	31	62	51	0.11
DQ-9	8/29	1.0	4	11	47	1	618	400	24	16	29	68	46	0.10
DQ-10	9/5	1.4	3	29	41	1	777	418	27	16	50	67	52	0.11
DQ-11	9/12	0.8	4	17	51	31	678	445	29	18	38	70	51	0.11
DQ-12	9/19	0.8	7	9	54	6	697	430	23	17	24	71	50	0.09
DQ-13	9/26	1.4	5	10	55	47	717	453	25	18	25	72	53	0.08
DQ-14	10/3	0.9	5	24	64	31	658	447	25	18	59	74	53	0.13
DQ-15	10/10	0.8	5	27	73	55	817	461	28	19	66	76	60	0.14
Upper Marsyandi (#4)														
UM-1	7/2	77.6	6	21	381	ND	1297	865	33	275	68	33	123	0.06
UM-2	7/10	99.6	7	33	379	ND	1457	888	39	266	80	35	130	0.06
UM-3	7/17	67.7	7	47	532	ND	1277	939	34	352	103	44	145	0.06
UM-4	7/24	82.0	6	58	521	ND	1517	931	39	339	137	39	151	0.08
UM-5	7/31	78.1	6	33	429	4	1557	972	32	292	80	39	142	0.05
UM-6	8/7	68.8	7	50	596	56	1417	992	32	395	113	50	160	0.06
UM-7	8/14	90.2	6	30	665	ND	1357	999	33	410	100	40	163	0.06
UM-8	8/21	99.6	5	27	573	ND	1377	958	31	351	84	39	151	0.06
UM-9	8/28	83.1	6	44	784	29	1577	1106	32	506	126	50	190	0.06
UM-10	9/4	80.9	5	34	634	ND	1297	954	28	405	100	45	156	0.06
UM-11	9/11	68.8	7	79	804	74	1617	1094	33	543	182	61	197	0.07
UM-12	9/18	71.5	8	51	725	51	1537	1062	30	517	121	63	182	0.05
UM-13	9/25	63.8	8	63	760	24	1657	1100	33	558	138	70	193	0.05
UM-14	10/2	50.6	8	75	764	ND	1996	1131	36	556	152	72	205	0.06

UM-15	10/9	42.4	8	85	803	ND	1836	1098	35	594	169	76	205	0.06
UM-16	10/16	34.1	9	135	829	ND	1776	1158	40	620	243	82	213	0.07
UM-17	10/23	31.9	9	123	783	4	2136	1127	38	600	220	83	217	0.07
Lower Marsyandi (#7)														
LM-1	7/3	105.3	9	31	476	ND	1297	797	28	198	68	42	129	0.05
LM-2	7/10	135.0	12	36	404	ND	1317	764	33	199	62	40	121	0.04
LM-3	7/17	92.4	12	34	407	ND	1097	819	31	254	87	47	119	0.06
LM-4	7/24	127.1	10	32	319	ND	1278	798	29	233	62	46	114	0.04
LM-5	7/31	105.3	10	39	430	1	1097	750	26	196	74	43	117	0.05
LM-6	8/7	89.0	10	41	484	ND	1257	809	26	260	82	50	131	0.04
LM-7	8/14	112.6	10	41	484	ND	1277	825	25	284	105	44	133	0.06
LM-8	8/21	151.8	8	28	431	4	1097	822	27	248	75	43	121	0.05
LM-9	8/28	105.3	10	37	572	31	1197	893	26	343	94	53	144	0.05
LM-10	9/4	94.1	12	70	613	37	1177	820	24	291	82	49	144	0.02
LM-11	9/11	67.2	12	52	529	53	1357	939	29	397	144	70	151	0.07
LM-12	9/18	72.2	13	73	524	24	1357	881	28	361	110	67	147	0.04
LM-13	9/25	57.1	14	73	486	15	1337	878	29	377	146	76	144	0.06
LM-14	10/2	44.8	15	81	558	9	1277	849	30	347	127	80	147	0.05
LM-15	10/9	39.2	14	110	559	24	1437	940	31	412	144	87	160	0.03
LM-16	10/16	28.0	16	114	564	3	1517	926	34	405	189	87	163	0.06
LM-17	10/23	24.6	15	103	527	11	1457	912	33	407	185	89	157	0.06
LM-18	10/30	17.4	10	24	297	ND	1557	974	37	426	171	96	138	0.10
Dudh (#5)														
D-1	7/2	29.0	31	55	92	ND	759	501	23	30	44	71	62	0.00
D-2	7/10	29.0	22	23	80	ND	912	504	61	53	103	67	67	0.15
D-3	7/17	15.1	24	30	87	2	817	505	19	43	60	66	62	0.05
D-4	7/24	27.3	25	41	75	6	897	554	22	38	84	84	67	0.07
D-5	7/31	29.0	21	24	76	1	877	491	17	37	49	62	61	0.05
D-6	8/7	24.9	21	32	79	ND	717	468	17	39	61	64	57	0.05
D-7	8/14	27.3	19	25	79	ND	877	508	17	38	49	55	62	0.04
D-8	8/21	39.4	18	19	64	ND	678	453	15	37	38	53	52	0.04
D-9	8/28	22.0	21	39	86	56	817	481	19	45	69	66	63	0.05
D-10	9/4	26.7	20	23	68	0	797	479	15	39	46	65	58	0.04
D-11	9/11	19.1	25	68	84	9	797	488	18	45	110	87	65	0.07
D-12	9/18	22.0	26	30	69	9	877	480	16	39	60	87	62	0.05
D-13	9/25	18.0	25	39	75	66	957	485	17	51	74	96	68	0.06
D-14	10/2	13.9	26	46	68	ND	937	484	19	45	87	94	66	0.07
D-15	10/9	9.3	30	56	73	56	957	511	21	47	104	106	71	0.08
D-16	10/16	7.5	27	89	167	9	1037	626	24	112	163	105	90	0.08
D-17	10/23	5.8	30	82	73	ND	997	524	22	43	152	108	74	0.10
D-18	10/30	5.2	30	83	83	0	1057	560	24	56	157	111	79	0.10
Dona (#6)														
DA-1	7/3	14.3	7	12	96	1	857	466	22	33	25	51	60	0.04
DA-2	7/10	12.2	7	14	96	1	737	479	25	30	31	56	57	0.04
DA-3	7/17	12.5	7	13	83	ND	478	455	21	32	28	54	47	0.04

(*continued on next page*)

Table 2 (*continued*)

Sample	Date	Discharge (m^3/sec)	F (M)	Cl (M)	SO_4 (M)	NO_3 (M)	HCO_3 (M)	Ca (M)	K (M)	Mg (M)	Na (M)	Si (M)	TDS[a] (mg/L)	X_{sil}[b] (eq%)
DA-4	7/24	19.0	6	8	82	1	737	456	20	28	18	52	54	0.03
DA-5	7/31	14.3	7	13	95	ND	678	512	22	38	31	61	57	0.04
DA-6	8/7	15.5	7	14	85	ND	757	470	21	31	27	57	56	0.04
DA-7	8/14	21.3	6	22	70	ND	717	426	19	26	50	51	52	0.06
DA-8	8/21	22.2	6	12	91	19	797	504	22	33	29	64	60	0.04
DA-9	8/28	15.5	8	13	92	1	817	490	21	36	29	63	60	0.04
DA-10	9/4	13.9	6	15	68	ND	877	457	21	33	33	58	58	0.04
DA-11	9/11	9.9	7	27	83	30	917	513	22	30	59	73	65	0.06
DA-12	9/18	12.5	11	13	84	1	917	530	22	32	34	75	65	0.04
DA-13	9/25	9.4	9	28	86	11	937	526	23	30	62	78	67	0.06
DA-14	10/2	7.6	7	21	80	ND	857	545	26	32	43	79	64	0.05
DA-15	10/9	5.5	9	15	86	11	997	555	23	30	34	82	69	0.04
DA-16	10/16	4.6	9	33	90	29	1017	559	26	32	74	83	72	0.07
DA-17	10/23	4.0	10	42	101	12	997	567	26	34	79	83	73	0.06
DA-18	10/30	3.5	9	21	91	ND	917	556	25	32	44	81	68	0.05
Khudi (#9)														
KH-1	6/28	21.6	3	31	58	1	697	256	50	106	77	142	53	0.27
KH-2	7/5	43.2	3	23	68	1	598	265	44	97	62	144	51	0.24
KH-3	7/12	41.4	2	17	53	1	658	250	42	103	52	130	49	0.23
KH-4	7/19	45.0	3	42	86	ND	678	266	48	116	102	143	57	0.29
KH-5	7/22	75.6	2	18	60	1	478	210	45	78	55	130	42	0.29
KH-6	7/24	61.8	3	23	49	2	598	234	56	71	54	101	44	0.29
KH-7	7/26	48.6	2	16	49	ND	598	274	44	112	61	147	49	0.24
KH-8	8/2	61.8	3	14	29	3	658	249	41	100	46	116	45	0.22
KH-9	8/8	35.4	3	19	42	ND	658	277	47	108	63	156	51	0.24
KH-10	8/16	48.6	3	15	33	ND	598	243	45	100	57	145	46	0.26
KH-11	8/23	61.8	2	20	36	ND	638	261	46	91	54	135	48	0.23
KH-12	8/30	35.4	2	39	46	ND	598	229	42	98	110	148	49	0.35
KH-13	9/6	34.2	3	22	35	ND	817	294	48	96	71	160	56	0.25
KH-14	9/13	23.4	3	36	50	1	638	242	47	104	110	154	51	0.35
KH-15	9/20	21.6	3	43	13	1	697	235	45	100	119	148	49	0.36
KH-16	9/27	31.2	2	50	6	3	618	203	55	80	123	126	44	0.44
KH-17	10/4	18.6	2	17	14	ND	678	235	45	100	62	153	47	0.27
KH-18	10/11	15.6	2	21	58	2	697	253	49	108	71	159	54	0.28
KH-19	10/18	13.2	3	49	30	2	658	266	48	111	128	152	52	0.34
KH-20	10/25	11.4	3	53	52	7	857	274	52	113	143	162	62	0.37
Bhulbule (#8)														
BH-1	6/28	157.5	10	131	235	1	1137	713	41	174	170	72	105	0.06
BH-2	7/5	171.7	10	92	219	ND	1237	731	41	162	125	69	104	0.06
BH-3	7/12	286.4	8	85	192	ND	1137	689	41	146	122	72	96	0.07
BH-4	7/19	182.3	8	121	215	ND	1117	678	43	155	182	79	101	0.09
BH-5	7/22	354.6	7	76	181	30	997	612	40	127	108	75	87	0.07
BH-6	7/26	186.6	8	104	227	1	1157	718	41	170	140	79	104	0.06

BH-7	8/2	282.1	5	67	145	ND	957	548	41	121	99	81	79	0.08
BH-8	8/9	182.3	8	121	251	29	1217	727	44	181	159	86	110	0.06
BH-9	8/16	197.8	7	100	266	16	1097	717	39	183	138	81	106	0.06
BH-10	8/23	310.0	7	80	285	5	977	680	36	188	116	83	101	0.06
BH-11	8/30	182.3	8	135	395	9	1177	813	41	264	213	90	130	0.08
BH-12	9/6	190.3	8	91	274	ND	1097	672	35	204	131	80	104	0.06
BH-13	9/13	157.5	9	166	310	1	1137	703	42	240	237	97	118	0.09
BH-14	9/20	133.9	9	188	360	38	1157	757	46	267	259	107	128	0.08
BH-15	9/27	146.9	8	166	272	1	1077	663	41	220	233	101	110	0.09
BH-16	10/4	120.3	9	195	333	26	997	739	48	267	237	112	120	0.06
BH-17	10/11	104.8	10	225	381	ND	1237	797	50	302	264	119	137	0.06
BH-18	10/18	97.3	10	282	360	1	1257	782	52	297	342	119	139	0.07
BH-19	10/25	88.0	11	316	388	5	1317	820	61	311	384	126	148	0.08
Rainwater			NA	9	2	0.5	20	8	5	1	10			

NA = not analyzed; ND = not detected.

[a] Total dissolved solids.

[b] Fraction of silicate ions to total ions (cf. Section 3.2).

the literature. Besides, averaging the Ca/Na ratios of all catchments yields a value of 0.45 which is very similar to the overall Ca/Na ratio of 0.41 that Quade et al. (2003) employed to account for the Nepalese lithology. Calculating chemical weathering rates with this averaged ratio does not yield significantly different trends from those based on individual ratios, as we subsequently discuss. Concerning the Mg fraction from silicate weathering, Mg/K was given preference over Mg/Na due to its smaller ratio range, from 0.1 to 0.7 versus 0.1 to 1.3 for the latter (Table 3). Averaging Mg/K over all basins results in a value of 0.39, comparable to the Mg/K ratio of 0.5 used by Galy and France-Lanord (1999). The fraction of silicate ions to total ions (X_{sil}, Table 2) is then determined on an equivalent basis as:

$$X_{sil} = (2Ca_s + 2Mg_s + Na_s + K_s)/(2Ca^* + 2Mg^* + Na^* + K^*) \quad (1)$$

This equivalent fraction is a measure of the magnitude of silicate weathering compared to carbonate weathering and the potential of the catchment to effectively withdraw CO_2 from the atmosphere.

In order to assess the propagated errors (err*) associated with the key parameters of this study (flux, yield, weathering rate) the following uncertainties are established: 10% error from the chemical analyses and 5% error in the measurement of catchment areas. In addition, we estimate a 20% error in discharge measurements with a mass balance approach. Because the flow past the monitoring station #7 should approximate the sum of the contributing flows (stations #1, 2, 3, 3b, 5, and 6; Fig. 1), the difference between the two provides a measure of the error in our discharge measurements (Gabet et al., 2008).

Accounting for all these uncertainties leads to an err* for any elemental flux and yield of 22% and 23%, respectively. Silicate weathering rates (SilWR) bear two additional potential errors. First, based on the arithmetic mean of the extreme values, a 60% error could exist in the Ca/Na and Mg/K ratios. Second, the error associated with the determination of the catchment area consisting exclusively of silicate bedrock is assumed to be 20%. Although the Annapurna region comprises heterogeneous lithologies, it has been well-mapped (Colchen et al., 1986; Searle and Godin, 2003), allowing the distinction between carbonate and silicate source areas. This was achieved by scanning and geo-referencing Colchen et al.'s (1986) lithological map with a Geographic Information System (GIS). The silicate and calc-silicate units were digitized and overlaid onto a 90-m Digital Elevation Model to calculate the surface areas of silicate rocks. Map areas were adjusted by slope angle to estimate the actual surface area. For the calc–silicate units, a sil:calc ratio of 7:3 for the bulk mineralogy was estimated through dissolution experiments and field observations. Altogether, our approach generates a provisory err* of 67% for SilWR – if based only on one element. As SilWR are calculated using 5 ions (Section 4.5), the overall err* is $\leqslant \pm 23\%$. Propagated errors of other rates have been determined analogously and are presented in Table 4.

Table 3
Chemical composition of suspended sediment taken at the monitoring stations; molar elemental ratios have been added.

wt.%	#1	#2	#3+3b	#4	#5+6	#7	#8	#9
SiO_2	67.1	70.3	58.4	69.3	73.4	70.6	72.4	69.2
TiO_2	0.7	0.6	1.1	0.7	0.2	0.5	0.5	0.7
Al_2O_3	13.6	14.0	18.3	13.9	14.3	14.3	13.5	13.7
FeO	3.7	3.9	7.8	4.0	1.0	3.0	2.7	5.0
MnO	0.0	0.0	0.2	0.0	0.0	0.0	0.0	0.1
MgO	2.4	1.2	3.2	1.7	0.5	1.3	1.2	2.8
CaO	1.7	0.9	3.3	1.2	1.5	1.5	1.5	2.0
Na_2O	1.5	1.6	2.7	1.5	3.8	2.5	2.5	1.7
K_2O	3.6	3.1	3.8	3.3	4.4	3.8	3.6	3.1
P_2O_5	0.1	0.1	0.1	0.1	0.2	0.1	0.1	0.1
Sum	94.4	95.8	98.7	95.7	99.3	97.6	98.1	98.4
Ca/Na	0.63	0.30	0.68	0.44	0.22	0.32	0.32	0.68
Mg/Na	1.25	0.57	0.91	0.91	0.11	0.38	0.37	1.30
Mg/K	0.51	0.29	0.64	0.40	0.10	0.25	0.26	0.70

4. RESULTS AND DISCUSSION

4.1. Carbonate weathering in the catchments

Because the differences between total anion (TZ^-) and cation (TZ^+) charges were $\leqslant$15% for the vast majority of the samples (and particularly of the trunk stream), the measured major ions account for most of the dissolved load (Fig. 2). Some samples from the tributaries display more varied normalized inorganic charge balances (NICB, calculated as $(TZ^+ - TZ^-)/TZ^+$), in exceptional cases as high as 38%. The principal reason for the consistent excess of TZ^+ over TZ^- is the lower alkalinity available to neutralize high Ca and Mg contents. The infrequent, but large charge imbalances cannot be explained by analytical errors, e.g., in the determination of alkalinity or by accidental contamination during field sampling. Fig. 2 shows the relationship between the discharge Q and the NICB. The solid lines have been added to illustrate that from the 30 samples with an NICB >15%, 29 display low discharges <50 m^3/s and those with an NICB $\geqslant$22% were sampled at even lower discharges of $\leqslant$17 m^3/s. Analytical inaccuracies as well as contaminations during the sampling procedure would not be affected by the discharge. This conspicuous relationship between Q and NICB therefore hints at the existence of a natural anion source, such as phosphate or organic matter that was not analyzed but showed a dilution/concentration effect. Given the location of the monitoring stations in the upper mountainous part of the Himalaya together with the very low measured nitrate concentrations and the fact that the very high NICB ($\geqslant$22%) occurs in four different watersheds in a comparably short time frame from 7/11 to 8/15, anthropogenic sources (fertilizers and detergents) seem unlikely. The observations are more consistent with a natural anion source, but this issue has not been investigated further. Note, that the significant NICB observed in this study is absent in Tipper et al. (2006) and other related studies (e.g., Galy and France-Lanord, 1999) because these

Table 4
Compiled weathering yields and carbon dioxide consumption rates for the Marsyandi and its tributaries (propagated errors are given in brackets).

Station	Basin #	CatWR[a] (±27%) ton/km²/y	SilWR[b] (±23%) ton/km²/y	Y_{TDS}[c] (±10%) ton/km²/y	CO_2-My[d] (±63%) kmol/km²/y	CO_2-ky[d] (±50%) kmol/km²/y
Temang	3	8.8	23.4	124	<u>113</u>	<u>284</u>
Nar	2	1.1	1.5	33	9	39
Koto M	1	6.9	10.2	180	84	225
Danaque	3b	7.1	20.3	108	<u>90</u>	<u>226</u>
Upper M	4	3.2	5.6	97	32	108
Lower M	7	1.6	3.7	70	<u>13</u>	<u>56</u>
Dudh	5	1.5	5.2	44	<u>8</u>	<u>50</u>
Dana	6	2.1	8.2	76	<u>10</u>	<u>68</u>
Khudi	9	20.1	56.4	187	261	641
Bhulbule M	8	3.4	9.3	101	27	115

[a] Silicate cation weathering rate (cf. Section 4.5).
[b] Silicate weathering rate (cf. Section 4.5).
[c] Yield based on the amount of total dissolved solids.
[d] -ky and -My describe mid- and long-term CO_2 fixation; underlined values are thought to represent genuine atmospheric carbon dioxide removal while all other numbers may potentially be overestimates (cf. Section 4.6).

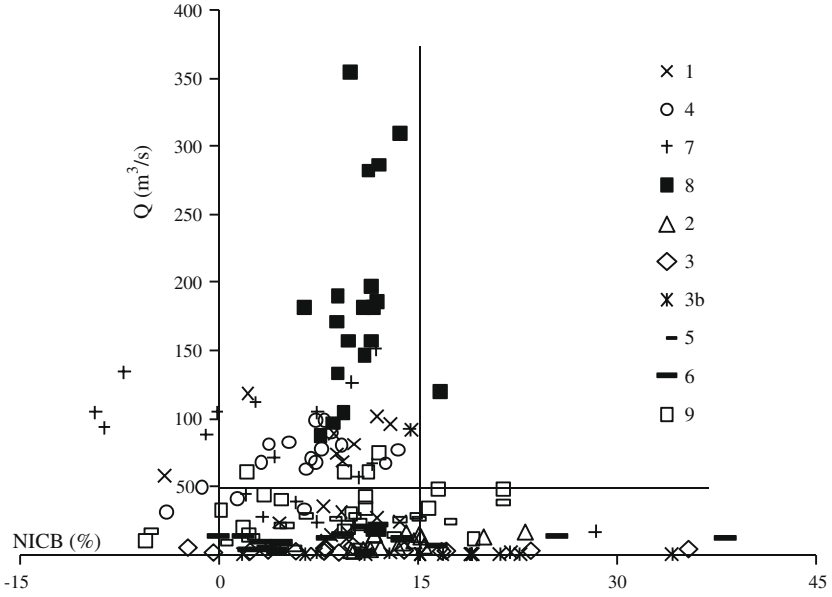

Fig. 2. Relationship between the discharge Q and the normalized inorganic charge balance NICB for all streams. The numbers in the legend represent the monitoring stations (#1, 4, 7, and 8 are from the trunk stream; all others are tributaries, cf. Table 1). For further explanation see Section 4.1.

sources determined alkalinity, with few exceptions, by charge balance, thus effectively suppressing any potentially indicative NICB.

For the purpose of differentiating between silicate and carbonate weathering and estimating CO_2 consumption rates in the Himalaya, the effect of the bedrock on Himalayan river chemistry has received special attention in the literature. The following studies all conclude that the solute load of trunk streams and tributaries in Himalayan drainage basins are chiefly characterized by a carbonate fingerprint (Sarin et al., 1989, 1992; Krishnaswami et al., 1992; Pande et al., 1994; Harris et al., 1998; Blum et al., 1998; Singh et al., 1998; Galy and France-Lanord, 1999; Pandey et al., 1999; Karim and Veizer, 2000; Jacobson and Blum, 2000; English et al., 2000; West et al., 2002; Dalai et al., 2002a; Jacobson et al., 2002; Oliver et al., 2003; Quade et al., 2003; Bickle et al., 2005; Tipper et al., 2006; Hren et al., 2007). An estimated 75–95% of the cations are derived from carbonate sources (e.g., Evans et al., 2004). The X_{sil} values in Table 2 as well as Fig. 3 corroborate this observation. The ternary plot of the solute cations reveals that watersheds draining the TSS and GHS (filled symbols) show $\leqslant$20% total alkali cations and a predominance of Ca and Mg, whereas those that include some Lesser Himalayan strata display a total alkali content of $\geqslant$16% and a less pronounced prevalence of Ca. In the corresponding anion plot bicarbonate is in general the most abundant anion and therefore complements the picture of catchments whose

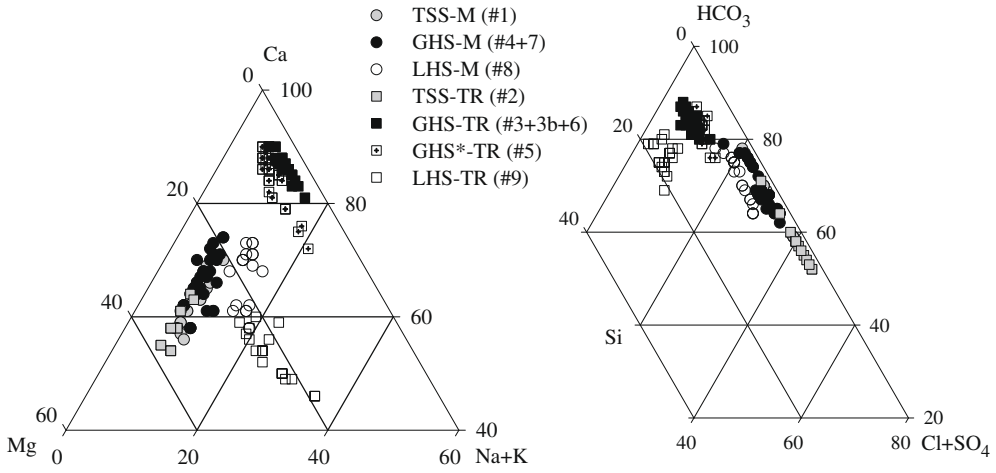

Fig. 3. Ternary graphs of major cations and anions of the different catchments. The prefixes in the legend represent the bedrock unit and the suffixes stand for Marsyandi (M) or tributary (TR).

river chemistry is primarily determined by carbonate weathering. The Marsyandi (all circles) carries the major ion chemistry derived from the TSS (TSS-M) throughout the GHS (GHS-M) without apparent contribution from the latter's lithology. Only upon entering the LHS does the Marsyandi's chemistry become richer in total dissolved solids (TDS) from silicate rocks (LHS-M). Because the total fluxes of the tributaries are significantly lower than those of the Marsyandi (Table 2), their differing chemical signatures (filled squares) are not appreciably transferred to the trunk stream. The tributaries draining the GHS (GHS-TR and GHS*-TR) are the rivers most conspicuously defined by dissolved limestone. However, while their anion content is indistinguishable, GHS*-TR, with headwaters in the Manaslu granite, exhibits a consistently higher proportion of Mg and, to a lesser extent, K. This contribution plausibly stems from the incongruent weathering of biotites in this granitic complex. Anderson et al. (1997, 2000) found preferential weathering of biotite in glacierized crystalline basins, consistent with this supposition. Note, that the source of the very low Mg concentrations for #3, 3b and 6 in Fig. 3 could be calcite itself and not necessarily silicates. Schneider and Masch (1993) reported up to 5 mol% $MgCO_3$ (~7 mol% Mg) in calcite grains of this study area.

Taking into account the predominantly silicate lithology in the GHS (A_{sil}/A_{tot} ratios between 71 and 86%, cf. Table 1), the quasi-exclusive carbonate chemistry of its tributaries #3, 3b, 5, and 6 seems unusual. Similarly, Blum et al. (1998) documented a watershed in the GHS (Raikhot) with 82% of the alkalinity flux derived from carbonate weathering in contrast to 18% from silicate weathering, despite a bedrock lithology consisting mostly of gneiss and granite with only ~1% carbonate. Their study, as well as the findings of White et al. (1999b) and Jacobson and Blum (2000) on the importance of disseminated calcite, suggests that the presence of small amounts of calcite in silicate bedrock suffice to establish the watershed's chemistry. An explanation for this observation is provided by Tipper et al. (2006) who reported that carbonate weathering is more sensitive to monsoonal runoff than silicate weathering due to its faster dissolution kinetics. Because the present study represents samples taken only during the monsoon season, it indeed appears that under high runoff/discharge conditions, carbonates, when present, are preferentially weathered over silicates. In addition to primary bedrock carbonates present as limestone or marble and the disseminated form of calcite occurring as fracture fillings and at grain boundaries, pedogenic calcite can also contribute to carbonate concentrations. Such pedogenic precipitates commonly occur during the dry season and become preferentially solubilized at the onset of the monsoon (Galy and France-Lanord, 1999). In our study area, however, no carbonate spike was evident in the early monsoon months. Also, Bickle et al. (2005) reasoned that secondary calcite deposited in soils and terraces adjacent to the streams is not likely to redissolve in the river waters as erosional transport of the substrate happens on a shorter time scale. Consequently, the very high Ca and bicarbonate concentrations in the tributaries are attributed to the *calc*-gneiss substrate as well as disseminated secondary calcite, which may have been more accessible to weathering.

4.2. Proton source in the TSS

The two rivers draining the TSS (#1 and 2) carry a considerable amount of sulfate, especially #2 (Fig. 3 and Table 2). Moreover, Mg and Ca concentrations of these streams vary linearly with the sulfate content (Fig. 4). The abundant presence of sulfate can have two origins: evaporite (gypsum) dissolution and/or sulfide oxidation. The fundamental difference in both processes is that the second one requires the supply of oxygen and releases protons as a by-product:

$$\mathbf{2}FeS_2(s) + 7.5O_2(aq) + 7H_2O(l) = \mathbf{4}SO_4^{2-}(aq) + 2Fe(OH)_3(s) + 8H^+ \quad (2)$$

The liberation of protons promotes chemical weathering but does not contribute to atmospheric CO_2 drawdown when released through pyrite oxidation. It is therefore crucial to attempt to determine the source of SO_4 in the TSS.

The correlation between sulfate and the alkaline earth metals in Fig. 4, with slopes considerably higher than unity can only be explained by evaporite dissolution under the premise of substantial subsequent precipitation of carbonates. Indeed, many literature sources report supersaturation of calcite (and also dolomite) in Himalayan river systems (cf. Jacobson et al., 2002) but our saturation calculations of the uncorrected raw data with PHREEQC (Parkhurst and Appelo, 1999) yield only partial supersaturation of the Marsyandi (#1 and 4) and the tributary TSS-TR (#2), and only with respect to calcite (Fig. 5). This supersaturation is a function of the discharge and water volume and manifests itself more markedly towards the end of the monsoon when the amount of TDS increases. Not surprisingly, the data with the highest TDS and lowest discharge were sampled in late October (Fig. 4, data points with gray fill and black outline). They are the only ones to display relatively low Ca values indicative of calcite precipitation and, as such, were not included in the regression of the data. But even assuming extended and sustained calcite precipitation (despite temporal undersaturation) the conspicu-

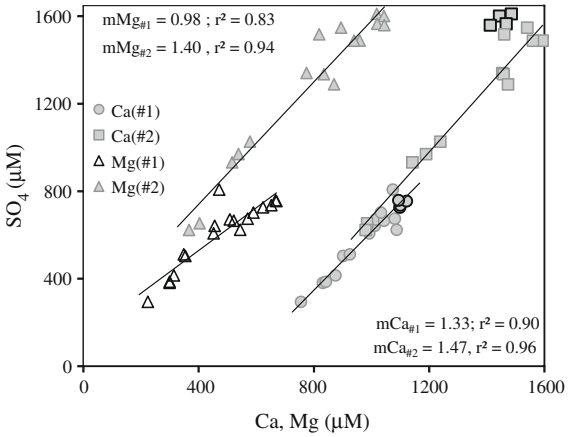

Fig. 4. Linearity between sulfate and the alkaline earths of the streams draining the TSS (#1 and #2, subscripted in the slopes '*m*'). Gray data points with black borders have been omitted in the regression (see Section 4.2).

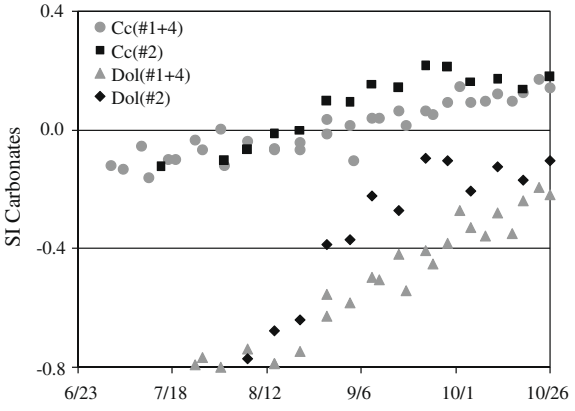

Fig. 5. Trend of the calcite (Cc) and dolomite (Dol) saturation indices (SI) over the sampling period which represents the entire monsoon season from June to October. Data are only shown for streams #2 and #1+#4 with headwaters in the TSS. These are the only rivers supersaturated with respect to carbonates.

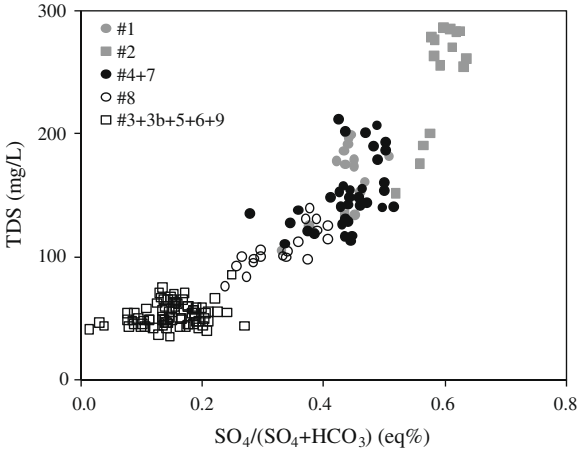

Fig. 6. Relationship between TDS and the ratio of $SO_4/(SO_4 + HCO_3)$ showing different patterns for mainstream and tributaries (open squares), respectively.

ous SO_4–Mg linearity in Fig. 4 does not support gypsum dissolution. Rather, it suggests that the protons released through pyrite oxidation liberate Mg, either from dolomite or (non-stoichiometrically) from a silicate source, such as biotite. Moreover, Hren et al. (2007) found a positive relationship between Cl and SO_4 in the Eastern Himalaya and inferred input from the weathering of evaporite minerals. However, our data lack any correlation between chloride and sulfate for the streams (data not shown). Besides, studies in this area of the Himalaya positively confirming and quantifying gypsum contribution to the stream chemistry are absent whereas the TSS includes black shales. Dalai et al. (2002b) successfully employed Re analysis to confirm sulfide oxidation from organic rich shales in the High Himalayas but, due to limited analytical Re resolution, our attempts at following their steps were inconclusive. If the sulfate fluxes of the TSS streams came exclusively from gypsum, it would require the annual dissolution of at least 32,000 m^3 of gypsum. It is unlikely that such considerable gypsum deposits have gone unnoticed so far. However, if the same river load stems from pyrite oxidation, the corresponding deposit volume is six times less.[3] Note that all these reflections are internally and externally consistent but present only circumstantial evidence. However, the mechanism of sulfide oxidation leading to the formation of sulfuric acid dissolving the bedrock was also proposed by Galy and France-Lanord (1999) to account for the high sulfate concentrations in TSS draining streams. By using $\delta^{13}C_{DIC}$ and introducing the ratio X_{SO4} $[SO_4/(SO_4+HCO_3)]$ these authors argued that the solute source of the Marsyandi in the TSS (datapoint NAG 24 in Fig. 6a from Galy and France-Lanord, 1999) is characterized by pure H_2SO_4 weathering of carbonates. The same combination of coupled sulfide oxidation and carbonate weathering has been proposed for other High Himalayan headwaters (e.g., Pandey et al., 1999; Hodson et al., 2002). The occurrence of the large amount of sulfate in the TSS headwaters in conjunction with potential carbonate precipitation yields a high X_{SO4} of ~0.6 for #2 (Fig. 6), similar to the value of 0.66 for NAG 24. Upon mixing with the Marsyandi, the sulfate component becomes diluted and the calcite precipitation diminishes, lowering X_{SO4}.

According to our reasoning in the previous section in combination with Eq. (2), chemical weathering in the TSS seems controlled by the amount of available oxygen which is needed to oxidize pyrite and thus generate protons. This, however, leads to a conundrum as the maximum sulfate concentration that can be obtained from sulfide oxidation using oxygen-saturated (glacial) water at high altitudes is less than 120 μmol/L[4]. This value is considerably lower than those observed in our study area (Fig. 4). We tentatively propose that the excess of sulfate and, therefore, oxygen comes from microbial activity (Skidmore et al., 2000), as suggested by stable-isotope studies of microbial processes in certain regions of the glacier bed (Bottrell and Tranter, 2002). Given that 10% of the TSS area is glaciated

[3] The daily sulfate fluxes (mol/d) were accumulated over the monsoon period yielding the overall sulfate load (mol), which was multiplied by the molar mineral volume (cm^3/mol) and converted into m^3. The molar volume of pyrite is only ⅓ that of gypsum (23.9 cm^3/mol, compared to 74.7 cm^3/mol) and only ½ mole of FeS_2 is required for every mole of SO_4 formed (Eq. (2)).

[4] The molar oxygen content of air-saturated water under normal atmospheric conditions at 25 °C is calculated based on the partial pressure of oxygen in the atmosphere (pO_2): 20.946 mol%·101,325 Pa = 21.223 kPa. Using Henry's law constant (k) of oxygen in water at 298 K (77.942 kPa L/mmol; www.henrys-law.org), its concentration becomes pO_2/k = 272 μmol/L. Henry's law constants decrease with decreasing temperature while increasing altitude lowers air and partial oxygen pressure. Based on an altitude of 5000 m and an air temperature of 2 °C (Table 1), air saturated surface/melt water draining the TSS is recalculated to have an equilibrated oxygen concentration of 221 μmol/L (using the barometric formula and an enthalpy of solution of 12.47 kJ/mol; www.henrys-law.org). As 7.5 O_2 produce 4 SO_4^{2-} (Eq. (2)), this corresponds to a stoichiometric sulfate concentration of 118 μmol/L.

(Table 1) and that the dominant reaction in subglacial environments is sulfide oxidation occurring in debris-rich environments (Tranter, 2003), the TSS samples may at least partially bear the chemical fingerprints of this glacierized environment. Despite the small proportion of glacierized terrain, this hypothesis is reinforced by Tranter et al. (2002) who found SO_4 values similar to those presented in Fig. 4 in a valley glacier bed in the Swiss Alps. The authors argued that, because oxidation of sulfides preferentially dissolves carbonates rather than silicates, only trace quantities ($\leqslant$0.7%) of carbonates and sulfides in silicate bedrock suffice to dissolve 5 times more carbonate than silicate. It is therefore conceivable that, rather than the presence of carbonates and shales as major constituents in the TSS, it is the presence of a subglacial environment with comminuted bedrock in contact with meltwater that causes the observed ion fluxes. These findings notwithstanding, it remains debatable whether this glacial process can *quantitatively* dominate the riverine signal given the dilution of glacial waters in the main river required to account for total runoff. There may be another, yet undiscovered oxygen source in the Himalayas leading to pyrite oxidation that does not require the crucial role of glaciers.

4.3. Silicate weathering in the catchments

The degree of silicate weathering in the respective catchments is illustrated by the ratio of Si/TDS versus $(Na_s + K_s)/TZ^+$ (Fig. 7). Complementary to the findings of the previous section, the catchments draining the TSS (gray symbols) exhibit very low Si/TDS ratios. As the Marsyandi expands to traverse the entire GHS, this ratio increases; however it is rather the TDS, which constantly decreases over the stations #4, #7 to #8 (Table 2 and Fig. 6) that contributes to the higher Si/TDS ratio of the trunk stream in Fig. 7. Overall, the Marsyandi picks up an additional ~50% Si during its journey across the GHS, of which the major fraction (37%) is contributed during the last leg between stations #7 and #8. A 60% increase in runoff from #7 to #8 as well as higher watershed temperatures in basin #8 may account for this disproportionate rise in the Si signal. The changing lithology in the LHS is unlikely to have caused this considerable rise in solute Si because only a small fraction of watershed #8 comprises LHS bedrock. Besides, the sampling location south of the MCT is still so close to the GHS that the substrate should not be much different from its northern counterpart.

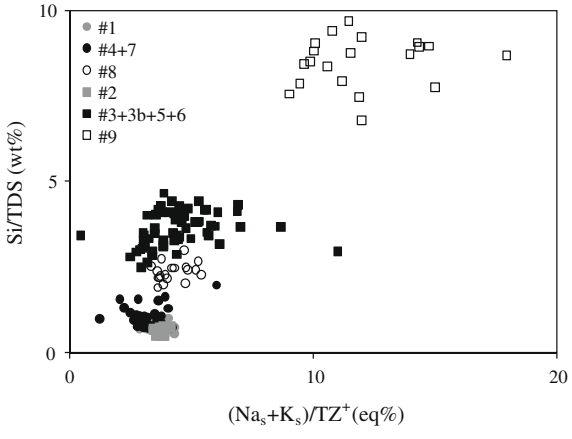

Fig. 7. Percent ratios of Si/TDS versus $(Na_s + K_s)/TZ^+$ indicate the magnitude of silicate weathering. The subscripted letter 's' ('silicate') and its derivation was introduced in Section 3.2.

The tributaries of the GHS display higher Si/TDS ratios than the Marsyandi, which is again based on the overall very low TDS in these catchments (Fig. 6). Their data form a relatively homogeneous cluster in Fig. 7 indicating that, despite their different geographic settings, the degree of silicate weathering is fairly similar in each. The exception to this generalization is basin #5 that exhibits Si concentrations more comparable to those of watershed #8 (Table 2). Both catchments display similar runoff and air temperatures but whereas #8 has by far the largest catchment area occupied by silicates in this study (A_{sil}, Table 1) to account for the high Si signal, the headwaters of #5 originate in the Manaslu granite and this felsic complex comprises a considerable part of the catchment area (Fig. 1). Yet, silicate weathering even in these two basins is not comparable at all to basin #9 which has the highest contribution from silicate sources (Fig. 7). Evans et al. (2001) found hot springs close to the MCT and estimated that 40% of their alkalinity originated from silicate weathering. Those authors inferred that hydrothermal activity presented an important source of silicate-derived alkalinity to the Marsyandi and its tributaries. This observation suggests that the enhanced silicate weathering in basin #9 might stem from hot spring contributions. However, it is basin #8 that primarily exhibits this hydrothermal influx and should therefore display the highest amount of additional cations and overall TDS. The average values of basin #8 indicate, by extension, that hydrothermal corrections as well as monsoonal dilution have also compensated for any potential hot spring silicate influx for #9. A more compelling cause for the increased silicate weathering in watershed #9 can rather be found in its low elevation and consequently higher air temperature (Table 1). The unusually high average runoff agrees with a distinct monsoonal rainfall maximum at 2100 m $\pm$ 300 m elevation found by Bookhagen and Burbank (2006) along the southern flank of the GHS. Whereas high runoff promotes kinetically limited weathering conditions that disfavor silicate dissolution, this inhibition may be partly compensated by the relatively thicker soils and denser vegetation at this elevation. These conditions enable the retention and percolation of water in the soil and increase the contact time between porewater and the minerals (Gabet et al., 2006). This view is supported by Tipper et al. (2006) who argued in favor of a greater proportion of silicate weathering, relative to carbonate weathering, during the dry season when the residence time of water in the ground increases.

4.4. Temperature dependence of silicate weathering

The kinetics of the dissolution process is temperature dependent with granitoid catchments exhibiting considerably higher apparent activation energies (Ea) than carbonates. Based on the silica flux, an Ea range of 49–59 kJ/mol is well established in the literature (White and Blum, 1995; White et al., 1999a; Dalai et al., 2002; Oliva et al., 2003). These energies are higher than those postulated for calcite and limestone hydrolysis (20 kJ/mol), derived from laboratory experiments (Alkattan et al., 1998). It follows that the warmer temperatures in basin #9 promote more silicate versus carbonate dissolution in comparison to all other watersheds. Given that altitude determines temperature and thus influences vegetation and soil formation, enhanced silicate weathering cannot be attributed to any of these parameters in particular: temperature determines kinetics, vegetation excretes organic acids supplying protons and ligands, and soil depth provides the necessary contact time. Of these factors, only the importance of temperature in chemical weathering processes can be illustrated in this study. When air temperatures are plotted against the yield of the principal silicate ions of every catchment (Fig. 8), all yields display a temperature dependence. This correlation becomes more conspicuous when omitting the yields from basin #3b (11 °C) which obscure the relationship between silicate weathering and climate, probably because of the very small watershed area (Table 1).[5] The temperature dependence is similar for the silicate cations (±parallel slopes in Fig. 8) and ~4-times greater for Si. This finding is consistent with the concept of incongruent release of the crystal network modifiers by diffusive leaching, a process less susceptible to temperature than hydrolysis of the silicate structure (e.g., Lasaga, 1998).

In a study on granitoid catchments, White and Blum (1995) found a similar temperature dependence for Na and Si as in Fig. 8 but no climatic correlation of K, Mg, and Ca. Those authors reasoned that, given their compilation of chemical analyses from 68 geographically different watersheds, interfering processes, such as nutrient cycling and variations in lithology, obscured any climatic signal. In contrast, our study area can be considered hydrologically as one large watershed with sparse vegetation and bioactivity which could affect the K, Mg, and Ca nutrient uptake. This combination may explain the strong climatic dependence reflected in the high correlation coefficients in Fig. 8.

The conspicuous temperature dependence of Si translates into an apparent activation energy (Ea) of 160 kJ/mol. Considering the commonly accepted Ea from laboratory mineral dissolution (20–80 kJ/mol; e.g., Brantley, 2003) and the watershed studies cited above, our Ea seems anomalously high, particularly because a recent study in a granitic watershed suggests an even lower apparent activation energy of 24 kJ/mol (Riebe et al., 2004a). Clearly, weathering encompasses many different interrelated processes and so, by extension, does the Si content of the fluid.

[5] Leaving out also the data for basin #3 with a similarly small catchment area does not alter the fit.

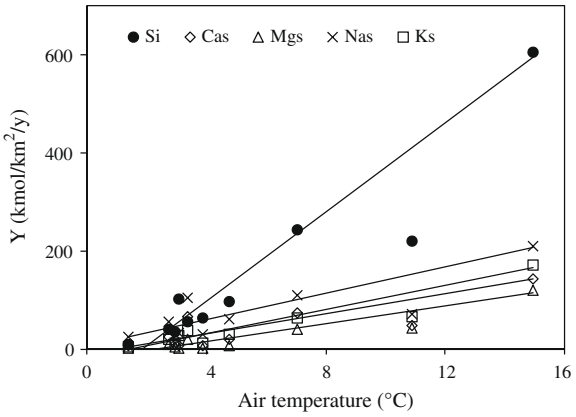

Fig. 8. Individual cation yields (Y) from silicate weathering as a function of the mean air temperature. Correlation coefficients of linear regressions of the individual yields are 0.98, 0.81, 0.95, 0.85, and 0.96 for Si, Ca_s, Mg_s, Na_s, and K_s, respectively (without basin #3b, see Section 4.4).

Moreover, temperature not only affects inorganic dissolution rates but also the solubility of minerals, thus altering the saturation indices of the minerals being dissolved or precipitated. Fluid flow rates can also change over time, as can elemental residence times as a function of the presence of organic matter (Oliva et al., 1999) and temperature. This discussion of the temperature dependence of silicate weathering may be further complicated by the confounding effects of climate and erosion because the warmest and wettest watersheds are also those eroding the fastest. Yet, although there is a relationship between monsoon rainfall and erosion rate in the Marsyandi basin (Gabet et al., 2008), no significant relationship was found between temperature and erosion rate. The absence of a relationship between these last two variables suggests that correlations between temperature and silicate weathering are, after all, not confounded by correlations between erosion and silicate weathering.

As to the variations in Ea derived from silica fluxes from granitoid watersheds, we suggest that dissolution and precipitation are mechanisms that are in general more temperature sensitive at lower temperatures than at higher ones. At low temperatures, back reactions involving Si are more relevant due to the lower solubility of potential precipitation phases. PHREEQC saturation calculations found that all watersheds of this study were already supersaturated with kaolinite at aqueous Al concentrations $\geqslant$110 nM. It is noteworthy that the oft-cited relationship between Si and Na (e.g., Hren et al., 2007), indicative of plagioclase-to-kaolinite weathering, is in general weak ($r^2 \leqslant 0.8$ for every catchment) and displays slopes ($\leqslant$0.5) requiring either the precipitation of another silica phase besides kaolinite or non-stoichiometric dissolution (graph not shown). With respect to dissolution, low temperature exerts a direct inhibitory influence (reducing the diffusion of protons in and out of the lattice) or an indirect one (reducing the activity of microorganisms). Riebe et al. (2004b) found unexpectedly steep declines in the fractions of chemical versus total denudation as a function of temperature. Their data could not

be modeled satisfactorily employing an Ea of 60 kJ/mol; instead, our analysis of their data suggests a hypothetical Ea of $\geqslant$320 kJ/mol. Riebe et al. (2004b) attributed the elevated apparent temperature sensitivity to additional factors, such as temperature-dependent changes in soil chemistry and soil microbiology. Drever and Zobrist (1992) likewise reported a remarkable sensitivity of silica weathering as a function of elevation in an Alpine altitude transect and estimated an Ea of ~180 kJ/mol. Despite the limitations of interpreting the meaning of apparent activation energies in terms of temperature-dependence of chemical weathering, the Ea inferred from Fig. 8 suggests that the disintegration of the silicate structure is reaction controlled. As non-stoichiometric silicate weathering is a feature of kinetically limited systems, with high runoff, short contact times, and glacial cover (Anderson et al., 1997; Hodson et al., 2000, 2002), we conclude that the catchments in the Upper Himalaya clearly fall into this classification.

4.5. Silicate weathering rates

The calculation of silicate weathering rates (SilWR) is a common way of estimating the degree of chemical denudation of silicate bedrock. However, established methods differ in their mode of calculation, thus making comparisons between diverse studies awkward. Some sources exclude silica in the computation of SilWR (e.g., Millot et al., 2002), whereas others include it but base their determinations on oxide instead of elemental masses (e.g., France-Lanord et al., 2003) or milli-equivalents (e.g., Hodson et al., 2002). As to the CO_2 consumption rate, this parameter is sometimes linked to the concentration of Ca and Mg (e.g., Berner et al., 2003) or just bicarbonate (e.g., Dessert et al., 2003) or Si (e.g., Huh et al., 1998). A further issue clouding the comparison of weathering and CO_2 consumption rates from different studies arises from the way discharges and yields are determined. Commonly, the mean annual runoff and the total catchment area are used. Whereas this approach is legitimate in rather uniform geological environments, such as continental sedimentary basins, cratons, or large igneous provinces, watersheds of varied lithology are more problematic, especially where no relationship exists between catchment size and the surface area of the silicate or carbonate bedrock. To overcome these inaccuracies, we normalized the solute fluxes according to the estimated surface areas of the carbonate and silicate bedrocks (see Section 3.2). Although this approach has its shortcomings (cf. Gaillardet et al., 1999), it is more appropriate than indiscriminately normalizing the solute flux to the total watershed area.

Weekly solute concentrations of the silica-derived major cations were multiplied by the discharge to determine solute fluxes. These fluxes were then integrated over the monsoon months to yield the seasonal load which was assumed to represent quantitatively 60% of the elemental load of a calendar year. This figure is based on estimates from Galy and France-Lanord (1999), reporting chemical denudation rates 3–6 times higher during the four months of monsoon than during the remaining months of dry season. This rough approximation was refined by Tipper et al. (2006) who gauged that the monsoonal silicate weathering flux of the Marsyandi contributes 50–70% to the annual silicate weathering flux. Consequently, fluxes and rates in this study were corrected and ultimately normalized to the GIS-derived silicate surface area, leading to the determination of silicate weathering rates according to:

$$\mathrm{SilWR} = (100/60) \cdot (Y_{\mathrm{Cas}} + Y_{\mathrm{Mgs}} + Y_{\mathrm{Nas}} + Y_{\mathrm{Ks}} + Y_{\mathrm{SiO2}}) \quad (3)$$

where Y is the yield (ton/km^2/y) of the subscripted cation released by silicate weathering. Omitting the silica term in this equation leads to the derivation of silicate cation weathering rates (CatWR), which are often included in discussions of chemical erosion (e.g., Gaillardet et al., 1999). Our calculated weathering rates and the TDS yield ($Y_{\mathrm{TDS}} = \Sigma Y_{\mathrm{i}}$, where i represents every ion in Table 2) are complemented by two CO_2 drawdown rates (Table 4). Note that CatWR, SilWR, and both CO_2 rates are normalized to the area underlain by silicates, A_{sil}, whereas Y_{TDS} (a proxy for the total chemical denudation) is standardized to the total area, A_{tot} (Table 1). CatWR vary from 1.1 to 20 ton/km^2/y, a range similar to the 1.3–38 ton/km^2/y given for the sub-basins of the vast Brahmaputra catchment in the eastern Himalaya (Singh et al., 2005). Excluding the data from basin #9, the range of CatWR shrinks to 1.1–8.8 ton/km^2/y (Table 4). Considering the catchments' locations in the High Himalaya and that all but three of the watersheds are glacierized, this range is in good agreement with the CatWR of 8–8.7 ton/km^2/y that Hodson et al. (2002) found for the Himalayan Batura Glacier basin. This range is also similar to the CatWR of 7 ton/km^2/y measured from the Himalayan Chhota-Shigri Glacier (Hasnain et al., 1989). More importantly, France-Lanord et al. (2003) derived CatWR from adjacent Central Nepal rivers (including the Marsyandi) between 6 and 7 ton/km^2/y, again in concert with our own data. Note that all these CatWR are close to a world average of ~5 ton/km^2/y (Gaillardet et al., 1999) and thus not extraordinary in the absolute amount of chemical denudation of silicate bedrock. Equally comparable (excepting #9) are the SilWR of this study (1–23 ton/km^2/y) with SilWR from other Himalayan basins (10–28 ton/km^2/y) reported by Krishnaswami et al. (1999) and Dalai et al. (2002a). It was stated above that the CatWR and SilWR of #9 are significantly higher than in the other basins because the warmer temperatures and higher precipitation promote abundant vegetation and relatively thicker soils in the LHS. At the higher sites (TSS and GHS), soils are thinner, more bedrock is exposed, and glaciers occupy the headwaters of the basins. On a global scale, the CatWR in Table 4 correspond well with data from granitoid and metasedimentary watersheds all over the world (0.35–6.4 ton/km^2/y), compiled by Millot et al. (2002). The only value in that compilation[6] that significantly exceeds the given range (16.7 ton/km^2/y) comes, most fittingly, from a warm (22 °C) and wet (3.7 m of annual

[6] The list of weathering rates from worldwide catchments assembled by West et al. (2005) can be alternatively applied with a similar outcome.

runoff) watershed. As such, it is similar in weathering magnitude and regime with #9 and supports the spatial jump in CatWR observed in this study.

4.6. CO_2 drawdown in the catchments

With regard to carbon dioxide consumption in the Himalayas, which has been considered crucial to the global climate during the Tertiary (Raymo, 1994), CO_2 consumption rates across most of the Marsyandi catchment are not extraordinary (Table 4). The first of the CO_2 rates is based on the molar CatWR and represents the fixation of carbon dioxide by silicate dissolution at the millennial time scale (CO_2-ky). At the time scale of 10^6 years, however, only Ca_s and Mg_s contribute to the burial of carbon dioxide via carbonate precipitation in the oceans (Berner et al., 2003). Na_s and K_s are removed from the oceans primarily as silicates, reversing the initial CO_2 drawdown (Mackenzie and Garrels, 1966). Hence, the second CO_2 rate (CO_2-My) was calculated by only summing the molar Ca_s and Mg_s yields. CO_2-ky and CO_2-My (except #9) are similar to values derived from worldwide (granitoid) watersheds (White and Blum, 1995; Gaillardet et al., 1999; Singh et al., 2005) and at least 3–5 times lower than those from basaltic lithologies (Dessert et al., 2003). In addition, the derivation of drawdown rates is founded on the postulate that silicate weathering occurs via carbonation of exclusively atmospheric carbon dioxide. However, as demonstrated earlier, sulfuric acid is the prevailing proton source in the TSS. Consequently, the upper Marsyandi (#1 and 4) and tributary #2 do not formally consume atmospheric carbon dioxide because little carbonic acid was involved in the dissolution of the (predominantly carbonatic) substrate. The same inference was drawn by Anderson et al. (2000) in a study on the chemical weathering of an Alaskan glacier where carbonate dissolution and sulfide oxidation accounted for 90% of the solute flux. Furthermore, hot springs in the vicinity of the MCT could have contributed metamorphic CO_2 to the streams #8 and 9 (Galy and France-Lanord, 1999; Evans et al., 2001). Unequivocal signs of hydrothermal input were detected in #8 and although corrections were applied to all of the basins, they do not include bicarbonate. As such, both CO_2 values provided for #8 and 9 may be overestimates; however, low Cl concentrations in the latter, even as the monsoon waned, argue against significant hydrothermal input. To further complicate the situation for the glacierized basins, ancient atmospheric CO_2 trapped in ice bubbles and organic carbon from bacterial activity at the glacier bed may have contributed to the bicarbonate concentration (Fairchild et al., 1994; Skidmore et al., 2000; Tranter et al., 2002). Both carbon sources create carbonic acid that promotes bedrock weathering but does not bind (present-day) atmospheric CO_2. To the contrary, saturation of meltwater with carbon dioxide from these sources effectively impedes actual climate-related sequestration of atmospheric CO_2 – at least until part of the carbon dioxide is either consumed in weathering reactions or released into the atmosphere. With this perspective in mind, only a thorough $\delta^{13}C$ study (cf. Galy and France-Lanord, 1999; Karim and Veizer, 2000; Singh et al., 2005) would help to identify the different carbon sources in order to calculate more accurate CO_2 drawdown rates. Despite this lack of information, the underlined CO_2 values in Table 4 are those less prone to non-atmospheric CO_2 'contamination' (no apparent shales in glaciated area, no hydrothermal influx) and thus present potentially more accurate approximations of actual atmospheric carbon dioxide fixation. Of this reduced group, three CO_2-My values lie well below a calculated world mean of 63 kmol/km^2/y, averaged over 51 global rivers compiled by Gaillardet et al. (1999).

4.7. Controls on chemical weathering

Presently, there is some debate about the fundamental controls on chemical weathering. Some studies (e.g., Sarin et al., 1989; White and Blum, 1995; Kump et al., 2000) have found that climate plays a critical role. These results have been used to support the hypothesis that chemical weathering and climate are coupled via a negative feedback process where increases in global temperature are tempered by concomitant increases in weathering rates (Walker et al., 1981; Berner et al., 2003). Alternatively, others have proposed that erosion, particularly the removal of chemically weathered material from the surface, is the dominant control such that an increase in erosion rate in the Himalayan region may have led to enhanced CO_2 sequestration and, thus, a decrease in global temperatures (Raymo and Ruddiman, 1992). To test this hypothesis, several studies have sought to define a relationship between erosion and chemical weathering. Data from field studies have shown a positive relationship between the two (Gaillardet et al., 1999; Riebe et al., 2001a,b, 2004a,b; Hren et al., 2007) although the relationship appears to be less than linear such that, at the high end of erosion rates, increases in erosion are not matched by increases in weathering (Millot et al., 2002; West et al., 2005; Gabet, 2007; Gabet and Mudd, 2009). The collection of suspended sediment issuing from the watersheds examined in the present study (Gabet et al., 2008), as well as the data from the meteorological stations, provides the opportunity to begin to investigate the controls on chemical weathering in the Himalayas.

In previous studies, TDS yields have been found to vary as a function of rainfall and relief (Sarin et al., 1989), basin area (Froehlich, 1983; Jha et al., 1988), and, most importantly, physical erosion (e.g., Anderson et al., 2002; Dupré et al., 2003; Quin et al., 2006). Our comparisons of Y_{TDS} and SilWR with climatic and geomorphic variables have been tabulated as least square regression coefficients in Table 5. We attribute the consistently low r^2 for Y_{TDS} to the high fraction of carbonate weathering ($1 - X_{sil}$) in the catchments (Table 2). Owing to its fast dissolution kinetics and ubiquity, carbonate weathering is equally unaffected by climate or relief, under kinetically limited as well as transport limited conditions. Support for this conclusion comes even from a study on low-elevation watersheds where Szramek et al. (2007) observed that calcite and dolomite dissolution kept pace with increasing river discharge, indicating that carbonate weathering is limited only by water flux and solubilities. Those authors concluded that global

fluxes of carbonate-related weathering products appear therefore heavily skewed toward carbonate-bearing environments with relatively low mean annual temperatures and high discharge, thus making a strong case for the High Himalaya during monsoon.

In contrast, SilWR appears sensitive to climate, as represented by runoff and temperature (Table 5). This observation is consistent with West et al. (2005) who propose that climatic factors determine the degree of chemical weathering under kinetically limited conditions. Accordingly, with the high erosion rates in the Himalayas (Gabet et al., 2008) supplying more fresh material, the weathering system shifts toward climate controlled conditions and temperature gains more importance. In addition to climate, SilWR also shows a correlation with physical erosion rates (PER, Table 5). In the warm and humid southern watersheds, landsliding is the dominant erosional mechanism and removal of the weathered regolith from the slopes exposes highly reactive fresh mineral surfaces (West et al., 2002; Gabet et al., 2004; Gabet, 2007). In the colder and drier northern watersheds where glaciers dominate the erosional regime (Gabet et al., 2008), grinding at the glaciers' beds creates fresh mineral surfaces (Anderson, 2005). Simple attempts to correlate erosion rate or climate with chemical weathering, however, are confounded by the observation that the warmest watersheds are also those that are eroding the fastest (Gabet et al., 2008). Furthermore, a lag between the arrival of the warmest temperatures and the arrival of the heaviest rainfall in the northern watersheds (Gabet et al., 2008) suggests that the dominant source of runoff and solutes shifts from glacial melt to hillslope runoff during the monsoon season. In light of these complexities, a thorough analysis of the controls on silicate weathering in the region will be presented in a follow-up contribution.

5. CONCLUSIONS

Our geochemical analysis generates the following coherent picture of weathering in the High Himalayas during the monsoon and its effect on climate. The low temperatures at high altitudes and the presence of glacial meltwater that enhance carbonate solubilities, the relatively high runoff during the monsoon, the intrinsically faster dissolution kinetics of carbonates and their abundance in the TSS, all these conditions ensure the prevalence of carbonate weathering in the Upper Himalaya. In addition, glacial activity appears to favor carbonate versus silicate weathering (Tranter, 2003) and even trace amounts of carbonates in felsic bedrock may suffice to account for the principal share of chemical weathering (Blum et al., 1998; White et al., 1999b; Jacobson and Blum, 2000; Anderson and Dietrich, 2001; Hren et al., 2007). Consequently, it is rather unexpected to still find up to 10% ions from silicate weathering in the Marsyandi River (cf. X_{sil}, Table 2). Mass balance considerations, constrained by $\delta^{13}C_{DIC}$, $\delta^{26}Mg$, $^{87}Sr/^{86}Sr$, and Re isotope data from related literature sources, suggest that streams with headwaters in the TSS reflect predominantly microbially mediated sulfide oxidation in glaciated areas leading to limestone weathering with carbonate precipitation only occurring at the end of the monsoon. Silicate weathering in the TSS is also driven by sulfuric acid dissolving comminuted material; otherwise, the low temperature of meltwater would have disfavored the considerably temperature dependent hydrolysis of silicate bedrock. As a consequence, silicate weathering from the trunk stream (bearing the chemical signature from the TSS downstream into the LHS) and the northern tributary #2 lead to only marginal rates of atmospheric CO_2 consumption. In the central part of the trunk stream course (#4, 7) the elemental composition does not change significantly because the tributaries feeding this part of the Marsyandi (#3, 3b, 5, 6) have lower discharges and TDS. With respect to the tributaries in the GHS, carbonate weathering is nearly as predominant as for the Marsyandi, with fractions from silicate weathering in general $\leqslant$15% and only exceptionally reaching 17 and 20%. Given the felsic and gneiss-rich lithology of the GHS, the solute chemistry is consistent with contributions from disseminated calcite. For the larger tributaries in the Greater Himalaya (watersheds #5 and 6), however, comminuted bedrock limestone may be the primary carbonate source because these watersheds exhibit the highest percentage of glaciated area in this study (Table 1). In the GHS, the primary proton source consists of $\sim\leqslant$80% of carbonic acid (estimated from Fig. 6). As such, silicate weathering consumes carbon dioxide. However, in only a few catchments can it be assumed that the CO_2 is entirely atmospheric in origin and from this reduced group only two watersheds (#3 and 3b) have CO_2-My consumption rates that are above the global average. From the group of catchments with less constrained carbon dioxide origin, the Khudi catchment (#9) in the southern Himalayan flank most effectively binds atmospheric CO_2 during weathering, after a small correction for potential metamorphic carbon dioxide contribution. This basin alone accounts for 50% of the CO_2-My flux in the studied Marsyandi basin. Considering that our study area is one of the wettest (Bookhagen et al., 2005) and fastest-eroding regions (Burbank et al., 2003; Blythe et al., 2007) in the High Himalayas, it should represent the high end of weathering rates in the range. Nevertheless, the average weathering rates over the entire basin are less than the global average, suggesting that the High Himalayas are not a significant sink of atmospheric carbon dioxide and that *in situ* chemical weathering does not influence the global climate. During the monsoon, however, higher suspended sediment fluxes from glacial erosion as well as landslides deliver material to the lowlands and plains, where silicate weathering markedly increases (France-Lanord et al., 2003). Additionally, suspended Ca flux was found to be more dependent on temperature and

Table 5
Regression coefficients (r^2) of least square linear regressions between climatic and geomorphic parameters and weathering surrogates (PER = physical erosion rates, taken from Gabet et al., 2008).

	Y_{TDS}	SilWR	PER
Temperature	<0.5	0.87	0.87
Runoff	<0.5	0.97	0.90
Relief	<0.5	<0.2	<0.2
A_{tot}, A_{sil}	<0.5	<0.2	<0.2

runoff than dissolved Ca flux (Gislason et al., 2006). These observations indicate that the net effect on global climate in the Himalayan basins may be through considerable physical erosion in the upper regions causing the silicate particles to be transported and thoroughly weathered in the lower regions. To the extent that sparsely vegetated, high-altitude crystalline terrains are characterized by extremely low silicate weathering under transport limited conditions (Riebe et al., 2004b) this would effectively result in no chemical exhumation for ⅔ of the year in such a cold and otherwise dry climate.

ACKNOWLEDGMENTS

We thank A. Duvall, B. Pratt-Sitaula, and A. Johnstone for field help, W. Amidon for map analysis, D. Anderson for XRD analysis, and S. Anderson, R. Berner, A. Blum, J. Blum, S. Brantley, and S. Gislason for discussions. This paper benefited greatly from instructive comments by the AE Krishnaswami and three anonymous reviewers. We are also grateful for AE Krishnaswami's help and patience in guiding this manuscript through the publication process. This research was funded by the National Science Foundation Continental Dynamics Program (Grant EAR-9909647) and by the National Aeronautics and Space Administration (NAGS-7781, NAGS-9039, and NAGS-10520). Logistical support from Himalayan Experience and the Nepalese Department of Hydrology and Meteorology is gratefully acknowledged.

REFERENCES

Alkattan M., Oelkers E. H., Dandurand J.-L. and Schott J. (1998) An experimental study of calcite and limestone dissolution rates as a function of pH from −1 to 3 and temperature from 25 to 80 °C. *Chem. Geol.* **151**, 199–214.

Amiotte-Suchet P., Probst J.-L. and Ludwig W. (2003) Worldwide distribution of continental rock lithology: implications for the atmospheric/soil CO_2 uptake by continental weathering and alkalinity river transport to the oceans. *Global Biogeochem. Cycles* **17**, 1038.

Anderson S. P. (2005) Glaciers show direct linkage between erosion rate and chemical weathering fluxes. *Geomorphology* **67**, 147–157.

Anderson S. P. and Dietrich W. E. (2001) Chemical weathering and runoff chemistry in a steep headwater catchment. *Hydrol. Process.* **15**, 1791–1815.

Anderson S. P., Drever J. I. and Humphrey N. F. (1997) Chemical weathering in glacial environments. *Geology* **25**, 399–402.

Anderson S. P., Drever J. I., Frost C. D. and Holden P. (2000) Chemical weathering in the foreland of a retreating glacier. *Geochim. Cosmochim. Acta* **64**, 1173–1189.

Anderson S. P., Dietrich W. E. and Brimball, Jr., G. H. (2002) Weathering profiles, mass-balance analysis, and rates of solute loss: linkages between weathering and erosion in small, steep catchements. *GSA Bull.* **114**, 1143–1158.

Berner E. K., Berner R. A. and Moulton K. L. (2003) Plants and mineral weathering: present and past. In *Surface and ground water, weathering, and soils* (ed. J. I. Drever). Treatise Geochem., vol. 5, pp. 169–188.

Bickle M. J., Chapman H. J., Bunbury J., Harris N. B. W., Fairchild I. J., Ahmad T. and Pomiès C. (2005) Relative contributions of silicate and carbonate rocks to riverine Sr fluxes in the headwaters of the Ganges. *Geochim. Cosmochim. Acta* **69**, 2221–2240.

Blum J. D., Gazis C. A., Jacobson A. D. and Chamberlain C. P. (1998) Carbonate versus silicate weathering in the Raikhot watershed within the High Himalayan Crystalline Series. *Geology* **26**, 411–414.

Bluth G. J. S. and Kump L. R. (1994) Lithologic and climatologic controls of river chemistry. *Geochim. Cosmochim. Acta* **58**, 2341–2359.

Blythe A. E., Burbank D. W., Carter A., Schmidt K. and Putkonen J. (2007) Plio-Quaternary exhumation history of the central Nepalese Himalaya: 1. Apatite and zircon fission track and apatite [U–Th]/He analyses. *Tectonics* **26**, TC3002. doi:10.1029/2006TC001990.

Bookhagen B. and Burbank D. W. (2006) Topography, relief, and TRMM-derived rainfall variations along the Himalaya. *Geophys. Res. Lett.* **33**, L08405.

Bookhagen B., Thiede R. C. and Strecker M. R. (2005) Abnormal monsoon years and their control on erosion and sediment flux in the high, arid northwest Himalaya. *Earth Planet. Sci. Lett.* **231**, 131–146.

Bottrell S. H. and Tranter M. (2002) Sulphide oxidation under partially anoxic conditions at the bed of Haut Glacier d'Arolla, Switzerland. *Hydrol. Process.* **16**, 2363–2368.

Brantley S. L. (2003) Reaction kinetics of primary rock-forming minerals under ambient conditions. In *Surface and ground water, weathering, and soils* (ed. J. I. Drever). Treatise Geochem., vol. 5, pp. 207–223.

Burbank D. W., Blythe A. E., Putkonen J., Pratt-Sitaula B., Gabet E., Oskin M., Barros A. and Ojha T. P. (2003) Decoupling of erosion and precipitation in the Himalayas. *Nature* **426**, 652–655.

Colchen M., Le Fort P. and Pêcher A. (1986). *Annapurna–Manaslu–Ganesh Himal.* , pp. 75–136.

Dalai T. K., Krishnaswami S. and Sarin M. M. (2002a) Major ion chemistry in the headwaters of the Yamuna river system: chemical weathering, its temperature dependence and CO_2 consumption in the Himalaya. *Geochim. Cosmochim. Acta* **66**, 3397–3416.

Dalai T. K., Singh S. K., Trivedi J. R. and Krishnaswami S. (2002b) Dissolved rhenium in the Yamuna River System and the Ganga in the Himalaya: role of black shale weathering on the budgets of Re, Os, and U in rivers and CO_2 in the atmosphere. *Geochim. Cosmochim. Acta* **66**, 29–43.

Das A., Krishnaswami S., Sarin M. M. and Pande K. (2005) Chemical weathering in the Krishna Basin and Western Ghats of the Deccan Traps, India: rates of basalt weathering and their controls. *Geochim. Cosmochim. Acta* **69**, 2067–2084.

Dessert C., Dupré B., François L. M., Schott J., Gaillardet J., Chakrapani G. and Bajpai S. (2001) Erosion of Deccan Traps determined by river geochemistry: impact on the global climate and the $^{87}Sr/^{86}Sr$ ratio of seawater. *Earth Planet. Sci. Lett.* **188**, 459–474.

Dessert C., Dupré B., Gaillardet J., François L. M. and Allègre C. J. (2003) Basalt weathering laws and the impact of basalt weathering on the global carbon cycle. *Chem. Geol.* **202**, 257–273.

Drever J. I. and Zobrist J. (1992) Chemical weathering of silicate rocks as a function of elevation in the southern Swiss Alps. *Geochim. Cosmochim. Acta* **56**, 3209–3216.

Dupré B., Dessert C., Oliva P., Goddéris Y., Viers J., François L. M., Millot R. and Gaillardet J. (2003) Rivers, chemical weathering and Earth's climate. *C.R. Geoscience* **335**, 1141–1160.

Edmond J. M., Palmer M. R., Measures C. I., Brown E. T. and Huh Y. (1996) Fluvial geochemistry of the eastern slope of the northeastern Andes and its foredeep in the drainage of the

Orinoco in Columbia and Venezuela. *Geochim. Cosmochim. Acta* **60**, 2949–2976.

English N. B., Quade J., DeCelles P. G. and Garzione C. N. (2000) Geologic control of Sr and major element chemistry in Himalayan Rivers, Nepal. *Geochim. Cosmochim. Acta* **64**, 2549–2566.

Evans M. J., Derry L. A. and France-Lanord C. (2004) Geothermal fluxes of alkalinity in the Narayani river system of central Nepal. *Geochem. Geophys. Geosyst.* **5**, Q08011.

Evans M. J., Derry L. A., Anderson S. P. and France-Lanord C. (2001) Hydrothermal source of radiogenic Sr to Himalayan rivers. *Geology* **29**, 803–806.

Fairchild I. J., Bradby L., Sharp M. and Tison J.-L. (1994) Hydrochemistry of carbonate terrains in alpine glacial settings. *Earth Surf. Process. Landforms* **19**, 33–54.

France-Lanord C. and Derry L. A. (1997) Organic carbon burial forcing of the carbon cycle from Himalayan erosion. *Nature* **390**, 65–67.

France-Lanord C., Evans M., Hurtrez J.-E. and Riotte J. (2003) Annual dissolved fluxes from Central Nepal rivers: budget of chemical erosion in the Himalayas. *C.R. Geoscience* **335**, 1131–1140.

Froehlich W. (1983) The mechanisms of dissolved solid transport in flysch drainage basins. *IAHS Publ.* **141**, 99–108.

Gabet E. J. (2007) A coupled chemical weathering and physical erosion model for a landslide-dominated landscape. *Earth Planet. Sci. Lett.* **264**, 259–265.

Gabet E. J. and Mudd S. M. (2009) A theoretical model coupling chemical weathering rates with denudation rates. *Geology* **37**, 151–154.

Gabet E. J., Burbank D. W., Putkonen J. K., Pratt-Sitaula B. A. and Ojha T. (2004) Rainfall thresholds for landsliding in the Himalayas of Nepal. *Geomorphology* **63**, 131–143.

Gabet E. J., Edelman R. and Langner H. (2006) Hydrological controls on chemical weathering at the soil-bedrock interface. *Geology* **34**, 1065–1068.

Gabet E. J., Burbank D. W., Pratt-Sitaula B. A., Putkonen J. K. and Bookhagen B. (2008) Modern erosion rates in the High Himalayas of Nepal. *Earth Planet. Sci. Lett.* **267**, 482–494.

Gaillardet J., Dupré B., Allègre C. J. and Négrel P. (1997) Chemical and physical denudation in the Amazon River Basin. *Chem. Geol.* **142**, 141–173.

Gaillardet J., Dupré B., Louvat P. and Allègre C. J. (1999) Global silicate weathering and CO_2 consumption rates deduced from the chemistry of large rivers. *Chem. Geol.* **159**, 3–30.

Galy A. and France-Lanord C. (1999) Weathering processes in the Ganges–Brahmaputra basin and the riverine alkalinity budget. *Chem. Geol.* **159**, 31–60.

Galy A. and France-Lanord C. (2001) Higher erosion rates in the Himalaya: geochemical constraints on riverine fluxes. *Geology* **29**, 23–26.

Gerlach T. (1991) Etna's greenhouse pump. *Nature* **351**, 352–353.

Gislason S. R., Oelkers E. H. and Snorrason A. (2006) Role of river-suspended material in the global carbon cycle. *Geology* **34**, 49–52.

Gleeson T. P. and Godin L. (2006) The Chako antiform: a folded segment of the Greater Himalayan sequence, Nar valley, Central Nepal Himalaya. *J. Asian Earth Sci.* **27**, 717–734.

Harris N., Bickle M., Chapman H., Fairchild I. and Bunbury J. (1998) The significance of Himalayan rivers for silicate weathering rates: evidence from the Bhote Kosi tributary. *Chem. Geol.* **144**, 205–220.

Hasnain S. I., Subramanian V. and Dhanpal K. (1989) Chemical characteristics and suspended sediment load of meltwaters from a Himalayan glacier in India. *J. Hydrol.* **106**, 99–108.

Hodges K. V., Wobus C., Ruhl K., Schildgen T. and Whipple K. (2004) Quaternary deformation, river steepening, and heavy precipitation at the front of the Higher Himalayan ranges. *Earth Planet. Sci. Lett.* **220**, 379–389.

Hodson A., Tranter M. and Vatne G. (2000) Contemporary rates of chemical denudation and atmospheric CO_2 sequestration in glacier basins: an Arctic perspective. *Earth Surf. Process. Landforms* **25**, 1447–1471.

Hodson A., Porter P., Lowe A. and Mumford P. (2002) Chemical denudation and silicate weathering in Himalayan glacier basins: Batura Glacier, Pakistan. *J. Hydrol.* **262**, 193–208.

Hren M. T., Chamberlain C. P., Hilley G. E., Blisniuk P. M. and Bookhagen B. (2007) Major ion chemistry of the Yarlung Tsangpo–Brahmaputra river: chemical weathering, erosion, and CO_2 consumption in the southern Tibetan plateau and eastern syntaxis of the Himalaya. *Geochim. Cosmochim. Acta* **71**, 2907–2935.

Huh Y, Tsoi M.-Y., Zaitsev A. and Edmond J. M. (1998) The fluvial geochemistry of the rivers of Eastern Siberia: I. Tributaries of the Lena River draining the sedimentary platform of the Siberian Craton. *Geochim. Cosmochim. Acta* **62**, 1657–1676.

Jacobson A. D. and Blum J. D. (2000) Ca/Sr and $^{87}Sr/^{86}Sr$ geochemistry of disseminated calcite in Himalayan silicate rocks from Naga Parbat: influence on river-water chemistry. *Geology* **28**, 463–466.

Jacobson A. D., Blum J. D. and Walter L. M. (2002) Reconciling the elemental and Sr isotope composition of Himalayan weathering fluxes: insights from the carbonate geochemistry of stream waters. *Geochim. Cosmochim. Acta* **66**, 3417–3429.

Jacobson A. D., Blum J. D., Chamberlain C. P., Craw D. and Koons P. O. (2003) Climatic and tectonic controls on chemical weathering in the New Zealand Southern Alps. *Geochim. Cosmochim. Acta* **67**, 29–46.

Jenkins A., Sloan W. T. and Cosby B. J. (1995) Stream chemistry in the middle hills and high mountains of the Himalayas, Nepal. *J. Hydrol.* **166**, 61–79.

Jha P. K., Subramanian V. and Sitasawad R. (1988) Chemical and sediment mass transfer in the Yamuna River – a tributary of the Ganges system. *J. Hydrol.* **104**, 237–246.

Karim A. and Veizer J. (2000) Weathering processes in the Indus River Basin: implications from riverine carbon, sulfur, oxygen, and strontium isotopes. *Chem. Geol.* **170**, 153–177.

Krishnaswami S. and Singh S. K. (1998) Silicate and carbonate weathering in the drainage basins of the Ganga–Ghaghara–Indus headwaters: contributions to major ion and Sr isotope geochemistry. *Proc. Indian Acad. Sci. (Earth Planet. Sci.)* **107**, 283–291.

Krishnaswami S., Trivedi J. R., Sarin M. M., Ramesh R. and Sharma K. K. (1992) Strontium isotopes and rubidium in the Ganga–Brahmaputra river system: weathering in the Himalaya, fluxes to the Bay of Bengal and contributions to the evolution of oceanic $^{87}Sr/^{86}Sr$. *Earth Planet. Sci. Lett.* **109**, 243–253.

Krishnaswami S., Singh S. K. and Dalai T. K. (1999) Silicate weathering in the Himalaya: role in contributing to major ions and radiogenic Sr to the Bay of Bengal. In *Ocean Science Trends and Future Directions* (ed. B. L. K. Somayajulu). Indian National Science Academy and Akademia International, New Delhi, pp. 23–51.

Kump L. R., Brantley S. L. and Arthur M. A. (2000) Chemical weathering, atmospheric CO_2, and climate. *Annual Rev. Earth Planet. Sci.* **28**, 611–667.

Lasaga A. C. (1998) *Kinetic Theory in the Earth Sciences*. Princeton University Press, New Jersey.

Lavé J. and Avouac J. P. (2001) Fluvial incision and tectonic uplift across the Himalayas of Central Nepal. *J. Geophys. Res.* **106**, 26561–26591.

Louvat P. and Allegre C. J. (1997) Present denudation rates on the island of Réunion determined by river geochemistry: basalt weathering and mass budget between chemical and mechanical erosions. *Geochim. Cosmochim. Acta* **61**, 3645–3669.

Lyons W. B., Carey A. E., Hicks D. M. and Nezat C. A. (2005) Chemical weathering in high-sediment-yielding watersheds, New Zealand. *J. Geophys. Res.* **110**, F01008.

Mackenzie F. T. and Garrels R. M. (1966) Chemical mass balance between rivers and oceans. *Am. J. Sci.* **264**, 507–525.

Millot R., Gaillardet J., Dupré B. and Allègre C. J. (2002) The global control of silicate weathering rates and the coupling with physical erosion: new insights from rivers of the Canadian Shield. *Earth Planet. Sci. Lett.* **196**, 83–98.

Moulton K. L., West J. and Berner R. A. (2000) Solute flux and mineral mass balance approaches to the quantification of plant effects on silicate weathering. *Am. J. Sci.* **300**, 539–570.

Oliva P., Viers J. and Dupré B. (2003) Chemical weathering in granitic environments. *Chem. Geol.* **202**, 225–256.

Oliva P., Viers J., Dupré B., Fortuné J. P., Martin F., Braun J. J., Nahon D. and Robain H. (1999) The effect of organic matter on chemical weathering: study of a small tropical watershed: Nsimi-Zoétélé site, Cameroon. *Geochim. Cosmochim. Acta* **63**, 4013–4035.

Oliver L., Harris N., Bickle M., Chapman H., Dise N. and Horstwood M. (2003) Silicate weathering rates decoupled from the $^{87}Sr/^{86}Sr$ ratio of the dissolved load during Himalayan erosion. *Chem. Geol.* **201**, 119–139.

Pande K., Sarin M. M., Trivedi J. R., Krishnaswami S. and Sharma K. K. (1994) The Indus river system (India–Pakistan): major-ion chemistry, uranium and strontium isotopes. *Chem. Geol.* **116**, 245–259.

Pandey S. K., Singh A. K. and Hasnain S. I. (1999) Weathering and geochemical processes controlling solute acquisition in Ganga Headwater–Bhagirathi River, Garhwal Himalaya, India. *Aquatic Geochem.* **5**, 357–379.

Parkhurst, D. L. and Appelo, C. A. J. (1999). User's guide to PHREEQC (Version 2) – A computer program for speciation, batch-reaction, one-dimensional transport, and inverse geochemical calculations. U.S. Geol. Surv. Water Resour. Inv. Report 99–4259.

Putkonen J. (2004) Continuous snow and rain data at 500 to 4400 m altitude near Annapurna, Nepal, 1999–2001. *Arc. Antarct. Alp. Res.* **36**, 244–248.

Quade J., English N. and DeCelles P. G. (2003) Silicate versus carbonate weathering in the Himalaya: a comparison of the Arun and Seti River watersheds. *Chem. Geol.* **202**, 275–296.

Quin J., Huh Y., Edmond J. M., Du G. and Ran J. (2006) Chemical and physical weathering in the Min Jiang, a headwater tributary of the Yangtze River. *Chem. Geol.* **227**, 53–69.

Raymo M. E. (1994) The Himalayas, organic carbon burial, and climate in the Miocene. *Paleoceanography* **9**, 399–404.

Raymo M. E. and Ruddiman W. F. (1992) Tectonic forcing of late Cenozoic climate. *Nature* **359**, 117–122.

Riebe C. S., Kirchner J. W., Granger D. E. and Finkel R. C. (2001a) Strong tectonic and weak climatic control of long-term chemical weathering rates. *Geology* **29**, 511–514.

Riebe C. S., Kirchner J. W., Granger D. E. and Finkel R. C. (2001b) Minimal climatic control on erosion rates in the Sierra Nevada, California. *Geology* **29**, 447–450.

Riebe C. S., Kirchner J. W. and Finkel R. C. (2003) Long-term rates of chemical weathering and physical erosion from cosmogenic nuclides and geochemical mass balance. *Geochim. Cosmochim. Acta* **67**, 4411–4427.

Riebe C. S., Kirchner J. W. and Finkel R. C. (2004a) Erosional and climatic effects on long-term chemical weathering rates in granitic landscapes spanning diverse climate regimes. *Earth Planet. Sci. Lett.* **224**, 547–562.

Riebe C. S., Kirchner J. W. and Finkel R. C. (2004b) Sharp decrease in long-term chemical weathering rates along an altitudinal transect. *Earth Planet. Sci. Lett.* **224**, 421–434.

Sarin M. M., Krishnaswami S., Dilli K., Somayajulu B. L. K. and Moore W. S. (1989) Major ion chemistry of the Ganga–Brahmaputra river system: weathering processes and fluxes to the Bay of Bengal. *Geochim. Cosmochim. Acta* **53**, 997–1009.

Sarin M. M., Krishnaswami S., Trivedi J. R. and Sharma K. K. (1992) Major ion chemistry of the Ganga source waters: weathering in the high altitude Himalaya. *Proc. Indian Acad. Sci. (Earth Planet. Sci.)* **101**, 89–98.

Schneider C. and Masch L. (1993) The metamorphism of the Tibetan Series from the Manang area Marsyandi Valley Central Nepal. In *Himalayan Tectonics*, vol. 74 (eds. M. P. Searle and P. J. Treloar). Geol. Soc. Special Publ., pp. 357–374.

Searle M. P. and Godin L. (2003) The South Tibetan Detachment Zone and the Manaslu Leucogranite: a structural reinterpretation and restoration of the Annapurna–Manaslu Himalaya, Nepal. *J. Geol.* **111**, 505–523.

Singh S. K., Trivedi J. R., Pande K., Ramesh R. and Krishnaswami S. (1998) Chemical and Strontium, Oxygen, and Carbon Isotopic Compositions of Carbonates from the Lesser Himalaya: implications to the Strontium Isotope Composition of the Source Waters of the Ganga, Ghaghara, and the Indus Rivers. *Geochim. Cosmochim. Acta* **62**, 743–755.

Singh S. K., Sarin M. M. and France-Lanord C. (2005) Chemical erosion in the eastern Himalaya: major ion composition of the Brahmaputra and $\delta^{13}C$ of dissolved inorganic carbon. *Geochim. Cosmochim. Acta* **69**, 3573–3588.

Skidmore M. L., Foght J. M. and Sharp M. J. (2000) Microbial life beneath a high Arctic glacier. *Appl. Environ. Microbiol.* **66**, 3214–3220.

Stallard R. F. (1995) Relating chemical and physical erosion. In *Chemical Weathering Rates of Silicate Minerals*, vol. 31 (eds. A. F. White and S. L. Brantley). Min. Soc. Am. Rev. Min., pp. 543–564.

Stallard R. F. and Edmond J. M. (1983) Geochemistry of the Amazon 2. The influence of geology and weathering environment on the dissolved load. *J. Geophys. Res.* **88**, 9671–9688.

Szramek K., McIntosh J. C., Williams E. L., Kanduc T., Ogrinc N. and Walthers L. M. (2007) Relative weathering intensity of calcite versus dolomite in carbonate-bearing temperate zone watersheds: carbonate geochemistry and fluxes from catchments within the St. Lawrence and Danube river basin. *Geochem. Geophys. Geosyst.* **8**, Q04002.

Tipper E. T., Bickle M. J., Galy A., West A. J., Pomiès C. and Chapman H. J. (2006) The short term climatic sensitivity of carbonate and silicate weathering fluxes: insight from seasonal variations in river chemistry. *Geochim. Cosmochim. Acta* **70**, 2737–2754.

Tranter M. (2003) Geochemical weathering in glacial and proglacial environments. In *Surface and Ground Water, Weathering, and Soils* (ed. J. I. Drever). Treatise Geochem., vol. 5, pp. 189–205.

Tranter M., Sharp M. J., Lamb H. R., Brown G. H., Hubbard B. P. and Willis I. C. (2002) Geochemical weathering at the bed of Haut Glacier d'Arolla, Switzerland – a new model. *Hydrol. Process.* **16**, 959–993.

Upreti B. N. (1999) An overview of the stratigraphy and tectonics of the Nepal Himalaya. *J. Asian Earth Sci.* **17**, 577–606.

Velbel M. A. (1993) Temperature dependence of silicate weathering in nature; how strong a negative feedback on long-term

accumulation of atmospheric CO_2 and global greenhouse warming? *Geology* **21**, 1059–1062.

Walker J. C. G., Hays P. B. and Kasting J. F. (1981) A negative feedback mechanism for the long-term stabilization of Earth's surface temperatures. *J. Geophys. Res.* **86**, 9776–9782.

West A. J., Bickle M. J., Collins R. and Brasington J. (2002) Small-catchment perspective on Himalayan weathering fluxes. *Geology* **30**, 355–358.

West A. J., Galy A. and Bickle M. (2005) Tectonic and climatic controls on silicate weathering. *Earth Planet. Sci. Lett.* **235**, 211–228.

White A. F. and Blum A. E. (1995) Effects of climate on chemical weathering in watersheds. *Geochim. Cosmochim. Acta* **59**, 1729–1747.

White A. F., Blum A. E., Bullen T. D., Vivit D. V., Schulz M. and Fitzpatrick J. (1999a) The effect of temperature on experimental and natural chemical weathering rates of granitoid rocks. *Geochim. Cosmochim. Acta* **63**, 3277–3291.

White A. F., Bullen T. D., Vivet D. V., Schulz M. and Chow D. W. (1999b) The role of disseminated calcite in the chemical weathering of granitoid rocks. *Geochim. Cosmochim. Acta* **63**, 1939–1953.

Associate editor: S. Krishnaswami